PHYSICAL REVIEW D **90,** 015012 (2014)

Overcoming velocity suppression in dark-matter direct-detection experiments

Keith R. Dienes,[1,2,*] Jason Kumar,[3,†] Brooks Thomas,[4,‡] and David Yaylali[3,§]

[1]*Department of Physics, University of Arizona, Tucson, Arizona 85721, USA*
[2]*Department of Physics, University of Maryland, College Park, Maryland 20742, USA*
[3]*Department of Physics, University of Hawaii, Honolulu, Hawaii 96822, USA*
[4]*Department of Physics, Carleton University, Ottawa, Ontario K1S 5B6, Canada*

(Received 5 January 2014; published 14 July 2014)

Pseudoscalar couplings between Standard-Model quarks and dark matter are normally not considered relevant for dark-matter direct-detection experiments because they lead to velocity-suppressed scattering cross sections in the nonrelativistic limit. However, at the nucleon level, such couplings are effectively enhanced by factors of order $\mathcal{O}(m_N/m_q) \sim 10^3$, where m_N and m_q are appropriate nucleon and quark masses, respectively. This enhancement can thus be sufficient to overcome the corresponding velocity suppression, implying—contrary to common lore—that direct-detection experiments can indeed be sensitive to pseudoscalar couplings. In this work, we explain how this enhancement arises, and present a model-independent analysis of pseudoscalar interactions at direct-detection experiments. We also identify those portions of the corresponding dark-matter parameter space which can be probed at current and future experiments of this type, and discuss the role of isospin violation in enhancing the corresponding experimental reach.

DOI: 10.1103/PhysRevD.90.015012 PACS numbers: 95.35.+d, 14.80.-j, 12.39.-x

I. INTRODUCTION

Among the many different experimental approaches towards understanding the particle nature of dark matter, direct-detection experiments are the only ones which directly probe the actual scattering of dark matter against ordinary Standard-Model (SM) matter. In general, such experiments seek to observe the infrequent scatterings of galactic-halo dark matter with atomic nuclei by searching for unambiguous evidence of the resulting nuclear recoils [1–4]. The discovery of such scattering events would arguably provide the most compelling possible evidence for the existence of dark matter, and would represent a major step towards the all-important goal of discerning the nature of the underlying dynamics that connects dark matter to the visible world.

That direct-detection experiments are capable of such powers of discernment is a direct consequence of the fact that different coupling structures between dark matter and ordinary Standard-Model matter yield significantly different scattering phenomenologies. As a result, any analysis of the experimental prospects for a given direct-detection experiment will inevitably rely on certain assumptions concerning the types of couplings that lead to this scattering. Since the interactions between the dark and visible sectors are by definition suppressed, one well-motivated possibility is that these two sectors are coupled by high-scale dynamics which gives rise to effective contact interactions at the energy scales relevant for direct detection. Although the consequences of couplings between dark matter and Standard-Model leptons have certainly been studied in the prior literature (see, e.g., Ref. [5]), it is far more common to consider elastic contact interactions between dark matter and SM quarks or gluons [2,3]. This preference is ultimately motivated by the recognition that direct-detection experiments are designed to capitalize on scattering between dark matter and atomic nuclei. In this paper we shall focus on couplings to quarks. Indeed, for a (Dirac) fermionic dark-matter particle χ, such contact interactions typically involve bilinear coupling structures of the form

$$(\bar{\chi}\Gamma\chi)(\bar{q}\Gamma' q), \tag{1.1}$$

where q denotes a Standard-Model quark and where Γ and Γ' represent different possible choices of Dirac gamma-matrix combinations $\{\mathbf{1}, i\gamma^5, \gamma^\mu, \gamma^\mu\gamma^5, \sigma^{\mu\nu}\}$. Different choices for Γ and Γ' correspond to different Lorentz and parity properties for the underlying interactions, and can thus lead to drastically different dark-matter phenomenologies (and therefore different predictions for associated event rates) at direct-detection experiments. For this reason, coupling structures which lead to attractive phenomenologies and greater event rates tend to be studied ubiquitously in the dark-matter literature, while those leading to suppressed event rates are typically neglected.

Unfortunately, by neglecting certain operators within this class, we are leaving many "stones unturned" in the hunt

*dienes@email.arizona.edu
†jkumar@hawaii.edu
‡bthomas@physics.carleton.ca
§yaylali@hawaii.edu

for dark matter. In particular, it may turn out that certain coupling structures which are seemingly suppressed (and thus are not considered) are actually enhanced by other factors. Such enhancements could conceivably overcome the apparent suppressions associated with these operators, implying that the contributions from such operators are not negligible after all.

In this work, we show that this is indeed the case for *pseudoscalar* coupling structures between dark matter and SM particles. The standard lore is that such coupling structures lead to direct-detection event rates which are suppressed relative to those associated with similar axial-vector coupling structures by factors of the χ/nucleus relative velocity $v \sim \mathcal{O}(10^{-3})$. However, one of the main points of this paper is to emphasize that there is a corresponding mitigating factor that can potentially overcome this velocity suppression: the process of transitioning from a fundamental pseudoscalar *quark* coupling to an effective pseudoscalar *nucleon* coupling introduces into the corresponding dark-matter scattering rate additional factors of order $\mathcal{O}(m_N/m_q) \sim 10^3$, where $m_{q,N}$ are the masses of the corresponding quarks and nucleons. Such enhancements, for example, are not present for axial-vector interactions, which are in some ways the closest cousins to the pseudoscalar interactions. In addition, we find that both axial-vector and pseudoscalar couplings are further enhanced in cases in which the dark-matter couplings are ultimately isospin-violating, with these enhancements becoming particularly striking in the case of pseudoscalar interactions. Thus, contrary to popular lore, we conclude that pseudoscalar couplings between dark matter and Standard-Model matter can indeed be probed at dark-matter direct-detection experiments.

This paper is organized as follows. First, we discuss the origins of the quark-to-nucleon enhancement factor that emerges for pseudoscalar interactions, and provide a careful analysis of the corresponding uncertainties that are inherent in such calculations. We also demonstrate that the possibility of isospin-violating pseudoscalar interactions only enhances these couplings further. We then proceed to present a model-independent analysis of pseudoscalar interactions at direct-detection experiments. In so doing, we also identify those portions of the corresponding dark-matter parameter space which can be probed at current and future experiments of this type.

II. FROM QUARKS TO NUCLEONS: VELOCITY SUPPRESSION AND NUCLEON ENHANCEMENT FOR PSEUDOSCALAR COUPLINGS

We begin by discussing the matrix elements and couplings that describe the contact interactions between fermionic dark matter and ordinary Standard-Model matter. This will also serve to introduce our notation and provide a point of comparison between interactions involving different Lorentz and parity structures. Ultimately, we shall focus on the cases of axial-vector and pseudoscalar interactions. It turns out that these two cases are closely related, yet have different resulting phenomenologies.

A. General preliminaries: Quark- and nucleon-level matrix elements and pseudoscalar velocity suppression

In general, we shall assume that our dark matter is a Dirac fermion χ whose dominant couplings to the visible sector are to Standard-Model quarks through dimension-six four-Fermi contact interactions described by Lagrangian operators of the bilinear form

$$\mathcal{O}_{\chi q}^{(XY)} = \frac{c_q^{(XY)}}{\Lambda^2}(\bar{\chi}\Gamma^X\chi)(\bar{q}\Gamma^Y q). \tag{2.1}$$

Here $q = u, d, s, \ldots$ specifies a particular species of quark, c_q is the corresponding χ/q coupling, and Λ corresponds to the mass scale of the new (presumably flavor-diagonal) physics which might generate such an effective interaction. The $\Gamma^{X,Y}$ factors are appropriate combinations of Dirac gamma matrices, with the X and Y indices ranging over the values $\{\mathrm{S}, \mathrm{P}, \mathrm{V}, \mathrm{A}, \mathrm{T}\}$ corresponding to $\Gamma^{(\mathrm{S})} \equiv \mathbf{1}$ (scalar interaction), $\Gamma^{(\mathrm{P})} \equiv i\gamma^5$ (pseudoscalar), $\Gamma^{(\mathrm{V})} \equiv \gamma^\mu$ (vector), $\Gamma^{(\mathrm{A})} \equiv \gamma^\mu\gamma^5$ (axial vector), and $\Gamma^{(\mathrm{T})} \equiv \sigma^{\mu\nu}$ (tensor), respectively. The form in Eq. (2.1) respects $U(1)_{\mathrm{EM}}$ and $SU(3)_{\mathrm{color}}$, as required, although $SU(2)_{\mathrm{weak}}$ is broken. This is appropriate for energy and momentum scales below the electroweak scale. The operator in Eq. (2.1) is also Lorentz invariant provided that X and Y are both chosen from the set $\{\mathrm{S}, \mathrm{P}\}$, the set $\{\mathrm{V}, \mathrm{A}\}$, or $\{\mathrm{T}\}$; note that in this last case, there are actually two ways in which the spacetime indices on each tensor can be contracted (either $\sigma_{\mu\nu}\sigma^{\mu\nu}$ or $\epsilon_{\mu\nu\lambda\rho}\sigma^{\mu\nu}\sigma^{\lambda\rho}$) when forming the Lorentz-invariant operator. In general, the operator $\mathcal{O}_{\chi q}^{(XY)}$ will be CP even in all Lorentz-invariant cases except when $XY = \mathrm{SP}$, PS, or TT with a contraction through the ϵ tensor.

In direct-detection experiments, these operators induce scattering between the dark-matter fermion χ and the individual nucleons N of the detector substrate. The tree-level matrix element describing this χ/N scattering is therefore given by

$$\mathcal{M}_{\chi N}^{(XY)} = \sum_q \frac{c_q^{(XY)}}{\Lambda^2}\langle\chi_f|\bar{\chi}\Gamma^X\chi|\chi_i\rangle\langle N_f|\bar{q}\Gamma^Y q|N_i\rangle, \tag{2.2}$$

where N denotes the particular nucleon species in question (either proton p or neutron n). Note that because the dark matter is a $U(1)_{\mathrm{EM}}$ singlet, N_i and N_f are both of the same species N and possibly differ only in their momenta and/or spins as the result of the scattering. The same will be assumed true for χ_i and χ_f, even in cases such as those in Refs. [6,7] in which the dark sector has multiple components.

In general, the nucleonic matrix element of the quark current $\bar{q}\Gamma^Y q$ cannot be evaluated analytically within a nucleonic background defined by N_i and N_f. Indeed, to do so would require a complete understanding of the manner in which the quark degrees of freedom are directly mapped onto those of the nucleon through the nonperturbative process of confinement. However, it is conventional to make the assumption that the nucleonic matrix element of the quark current is proportional to that of the corresponding *nucleon* current in the limit of vanishing momentum transfer [8–11]:

$$\langle N_f|\bar{q}\Gamma^Y q|N_i\rangle \equiv \Delta q^{(N)}\langle N_f|\bar{N}\Gamma^Y N|N_i\rangle, \tag{2.3}$$

where $\Delta q^{(N)}$ represents a fixed constant of proportionality that encapsulates the nonperturbative physics inherent in low-energy QCD. Indeed, this constant of proportionality is assumed to depend on the quark and nucleon in question, and also the specific choice of the Dirac-matrix structure Γ^Y involved, but is otherwise assumed to be independent of all other relevant variables (such as the particular spin and velocity configurations of the initial and final N_i and N_f states). In practice, the values of $\Delta q^{(N)}$ for the different relevant cases are calculated numerically through lattice gauge-theory techniques and/or extracted experimentally. We should emphasize, however, that the relation in Eq. (2.3) holds only as an approximate phenomenological "rule of thumb" and comes with several correction terms which can be taken to be small or even vanishing in various limits. Further details can be found in Ref. [9].

Given the numerical values of $\Delta q^{(N)}$ in Eq. (2.3), the rest of the matrix element (2.2) is now in a form which can be evaluated analytically. We then find

$$\mathcal{M}_{\chi N}^{(XY)} = \frac{g_{\chi N}}{\Lambda^2}\langle\chi_f|\bar{\chi}\Gamma^X\chi|\chi_i\rangle\langle N_f|\bar{N}\Gamma^Y N|N_i\rangle, \tag{2.4}$$

where the final dark-matter/nucleon coupling $g_{\chi N}$ is given by

$$g_{\chi N} \equiv \sum_q c_q^{(XY)}\Delta q^{(N)}. \tag{2.5}$$

In this paper, we shall be concerned with three particular Dirac-matrix bilinears: the scalar (S), the pseudoscalar (P), and the axial vector (A). In the nonrelativistic limit, the scalar bilinear matrix element behaves to leading order as

$$\text{S:}\quad \langle\psi_f|\bar{\psi}\psi|\psi_i\rangle \sim 2m_\psi(\xi_\psi^{s'})^\dagger\xi_\psi^s, \tag{2.6}$$

where ξ_ψ^s represents the two-component spinor corresponding to the fermion ψ with spin s, and where s and s' represent the spins of ψ_i and ψ_f respectively. By contrast, the corresponding pseudoscalar and axial-vector bilinear matrix elements behave to leading order as

$$\begin{aligned}
&\text{P:}\quad \langle\psi_f|\bar{\psi}\gamma^5\psi|\psi_i\rangle \sim (\xi_\psi^{s'})^\dagger[(\vec{p}_f-\vec{p}_i)\cdot\vec{\sigma}]\xi_\psi^s,\\
&\text{A:}\quad \begin{cases}\langle\psi_f|\bar{\psi}\gamma^0\gamma^5\psi|\psi_i\rangle \sim 0\\ \langle\psi_f|\bar{\psi}\vec{\gamma}\gamma^5\psi|\psi_i\rangle \sim 2m_\psi(\xi_\psi^{s'})^\dagger\vec{\sigma}\xi_\psi^s,\end{cases}
\end{aligned} \tag{2.7}$$

where $\vec{\sigma}$ are the Pauli spin matrices. Taking ψ to correspond to our nucleon field N, we thus see that both the pseudoscalar and axial-vector cases lead to a *spin-dependent* scattering amplitude to leading order. It is for this reason that the coefficients $\Delta q^{(N)}$ for these cases can be interpreted as characterizing the fraction of the spin of the nucleon N that is carried by the quark q. Indeed, in the case of pseudoscalar couplings, it is easy to show that *all* terms—and not just those at leading order—are spin dependent; this follows directly from the symmetry-based observation that any CP-odd Lorentz-scalar quantity which depends on only the properties of the nucleon must involve the nucleon spin [12–15]. On the other hand, we see that the pseudoscalar case also leads to a *velocity suppression*: the corresponding matrix element in Eq. (2.7) is proportional to the velocity transfer $\Delta\vec{v} \equiv \vec{v}_f - \vec{v}_i$, which is $\mathcal{O}(10^{-3})$ for most regions of interest involving dark-matter particles originating in the galactic halo. It is this velocity suppression which lies at the root of the relative disregard for pseudoscalar interactions in the dark-matter literature.

B. An enhancement factor for pseudoscalar matrix elements

Given these observations, our next task is to determine the numerical values of the $\Delta q^{(N)}$ coefficients for the different cases of interest. In this paper, our interest in the scalar coupling structure will be restricted to the dark-matter bilinear rather than the quark bilinear—i.e., in the language of Eq. (2.1) we will wish to consider the case with $X = \text{S}$, but never $Y = \text{S}$. Consequently, we shall only require the values of the coefficients $\Delta q^{(N)}$ for the axial-vector ($Y = \text{A}$) and pseudoscalar ($Y = \text{P}$) cases. We also emphasize that we are not merely interested in the "central values" of these coefficients; we are also interested in understanding their associated statistical and experimental *uncertainties*. As we shall see, it is only by keeping track of these uncertainties that we can make solid statements about the phenomenological consequences of the different couplings in each case.

Historically, the numerical values of the $\Delta q^{(N)}$ coefficients for the axial-vector case have been extracted through nucleon-structure scattering experiments [16–18] and through lattice gauge-theory calculations [19]. The results that we shall use in this paper are quoted in Table I, and represent the most current values taken from experiment and theory. In this context, it is important to note that there are rather significant uncertainties associated with the values of the $\Delta q^{(N)}$. While the measured values for $\Delta u^{(N)}$ and $\Delta d^{(N)}$ tend to agree reasonably well with results from lattice calculations, the values for $\Delta s^{(N)}$ obtained using these

TABLE I. Values used in this paper for the axial-vector coefficients $\Delta q^{(N)}$. The values for the $\Delta u^{(N)}$ and $\Delta d^{(N)}$ are taken from the recent lattice results reported in Ref. [19], while the values for the $\Delta s^{(N)}$ have been chosen such that they lie between these lattice results and the experimentally measured values in Ref. [18], roughly two standard deviations away from the central value obtained in each analysis.

	$N = p$	$N = n$
$\Delta u^{(N)}$	0.787 ± 0.158	-0.319 ± 0.066
$\Delta d^{(N)}$	-0.319 ± 0.066	0.787 ± 0.158
$\Delta s^{(N)}$	-0.040 ± 0.03	-0.040 ± 0.03

two methods can differ quite significantly. In this paper, we shall therefore adopt the $\Delta u^{(N)}$ and $\Delta d^{(N)}$ values quoted in Ref. [19], but choose values for the $\Delta s^{(N)}$ such that they lie between these lattice results and the experimentally measured values in Ref. [18], roughly two standard deviations away from the central value obtained in each analysis.

We also observe that the results quoted in Table I respect *quark-level* isospin invariance—i.e., they satisfy

$$\Delta u^{(p,n)} = \Delta d^{(n,p)}, \qquad \Delta s^{(p)} = \Delta s^{(n)}. \tag{2.8}$$

This makes sense, as the results in Table I are derived in the limit in which the three light quarks are considered to be effectively massless. Likewise, in this approximation, the remaining quarks are considered to be too heavy to contribute significantly to proton-level and neutron-level couplings. Thus, in the axial-vector case, we shall additionally take

$$\Delta c^{(p,n)} = \Delta b^{(p,n)} = \Delta t^{(p,n)} = 0. \tag{2.9}$$

We now turn to consider the corresponding coefficients in the pseudoscalar case. In order to distinguish these coefficients from the axial-vector coefficients above, we shall denote the pseudoscalar coefficients as $\Delta\tilde{q}^{(N)}$.

Rather than representing an independent degree of freedom, it turns out [20,21] that the pseudoscalar coefficients $\Delta\tilde{q}^{(N)}$ can actually be determined theoretically in terms of the axial-vector coefficients $\Delta q^{(N)}$. This is ultimately because a general axial-vector current $j^{\mu 5} \equiv \bar{\psi}\gamma^\mu\gamma^5\psi$ is not conserved in a theory in which $m_\psi \neq 0$, but is instead related to the pseudoscalar current $j^5 \equiv \bar{\psi} i\gamma^5\psi$ through a divergence relation of the form

$$\partial_\mu j^{\mu 5} = 2m_\psi j^5 + \frac{\alpha_s}{4\pi} G_{\mu\nu}\tilde{G}^{\mu\nu}, \tag{2.10}$$

where the final term reflects the possible additional contribution to the nonconservation of $j^{\mu 5}$ coming from a chiral anomaly (such as the chiral anomaly of QCD). Indeed, amongst all the fermion bilinears $\bar{\psi}\Gamma^Y\psi$ with which we started, it is only the axial-vector and pseudoscalar bilinears which can be connected to each other through such a direct relation.

It should be noted that in principle Eq. (2.10) also contains additional contributions resulting from integrating out light hadron states such as the pion. As discussed in Ref. [22], such a pion-induced additional contribution would appear as a pion pole term. However, this contribution is relatively small because the relevant momentum transfers for our analysis are in fact well below the pion mass. Indeed, since we are studying spin-dependent scattering, we will be focusing on experiments (such as COUPP [23]) which involve fluorine rather than xenon targets; the corresponding momentum transfers are then smaller because fluorine is lighter than xenon. Moreover, it is often the case within such experiments that events with large recoil energies are rejected due to the calibration difficulties that exist in this regime [24]. Thus, for all events of interest, the resulting momentum transfers are much smaller than in leading spin-independent direct-detection experiments, and we may disregard such pion-induced pole terms in what follows.

Exploiting Eq. (2.10) and following Ref. [20], we can now proceed to derive an expression for the pseudoscalar coefficients $\Delta\tilde{q}^{(N)}$ in terms of the axial-vector coefficients $\Delta q^{(N)}$. We begin by noting that

$$\begin{aligned} m_N \Delta q^{(N)} &\langle N_f|\bar{N} i\gamma^5 N|N_i\rangle \\ &= \frac{1}{2}\Delta q^{(N)}\partial_\mu\langle N_f|\bar{N}\gamma^\mu\gamma^5 N|N_i\rangle \\ &= \frac{1}{2}\partial_\mu[\Delta q^{(N)}\langle N_f|\bar{N}\gamma^\mu\gamma^5 N|N_i\rangle] \\ &= \frac{1}{2}\partial_\mu\langle N_f|\bar{q}\gamma^\mu\gamma^5 q|N_i\rangle \\ &= m_q\langle N_f|\bar{q} i\gamma^5 q|N_i\rangle + \frac{\alpha_s}{8\pi}\langle N_f|G\tilde{G}|N_i\rangle. \end{aligned} \tag{2.11}$$

In Eq. (2.11), the first equality follows from the current relation (2.10) in the nucleon-level theory, where (since all nucleons are color-neutral) no QCD chiral anomaly exists. The second equality, by contrast, follows from the fact that the $\Delta q^{(N)}$ coefficients are presumed to be constants without spacetime dependence, while the third equality follows from the definition of $\Delta q^{(N)}$ as relating the nucleon-level and quark-level axial-vector matrix elements. The final equality then again follows from Eq. (2.10), now evaluated in the quark-level theory for which the QCD chiral anomaly is nonzero.

For each nucleon N, the relation in Eq. (2.11) furnishes three constraint equations (one for each of the light quarks $q = u, d, s$). However, recognizing that our three desired coefficients $\Delta\tilde{q}^{(N)}$ are nothing but the ratios between the $\langle N_f|\bar{q} i\gamma^5 q|N_i\rangle$ and $\langle N_f|\bar{N} i\gamma^5 N|N_i\rangle$ matrix elements, we see that we still have one unknown remaining, namely the matrix element involving the QCD anomaly. An additional constraint equation is therefore called for. Towards this end,

it is traditional (see, e.g., Ref. [20]) to assume that the large-N_c chiral limit is a valid approximation. This then implies the additional constraint [25]

$$\langle N_f|\bar{u}\gamma^5 u|N_i\rangle + \langle N_f|\bar{d}\gamma^5 d|N_i\rangle + \langle N_f|\bar{s}\gamma^5 s|N_i\rangle = 0. \tag{2.12}$$

In principle, we could then proceed with this as our remaining constraint equation. However, the appeal to the large-N_c limit introduces a rather significant new source of uncertainties of order $\mathcal{O}(1/N_c)$ into our calculation. Since we wish to keep track of these uncertainties in this paper, we will ultimately need to find a way to parametrize the uncertainties inherent in the relation (2.12). We shall therefore write Eq. (2.12) in the modified form

$$\langle N_f|\bar{u}\gamma^5 u|N_i\rangle + \langle N_f|\bar{d}\gamma^5 d|N_i\rangle + \langle N_f|\bar{s}\gamma^5 s|N_i\rangle = \eta\langle N_f|\bar{N}\gamma^5 N|N_i\rangle, \tag{2.13}$$

where the right side of this equation is designed to reflect this uncertainty, with the numerical coefficient η assumed to have a vanishing central value but a relatively large uncertainty $\delta\eta \sim \mathcal{O}(1/N_c)$.

This system of equations (2.11) and (2.13) may now be solved for the coefficients $\Delta\tilde{q}^{(N)} \equiv \langle N_f|\bar{q}i\gamma^5 q|N_i\rangle / \langle N_f|\bar{N}i\gamma^5 N|N_i\rangle$ as well as an analogous anomaly coefficient

$$\Delta\tilde{G}^{(N)} \equiv \frac{\alpha_s}{8\pi}\frac{\langle N_f|G\tilde{G}|N_i\rangle}{\langle N_f|\bar{N}i\gamma^5 N|N_i\rangle}. \tag{2.14}$$

The results are then given by

$$\Delta\tilde{q}^{(N)} = \frac{m_N}{m_q}[\Delta q^{(N)} - X^{(N)}],$$
$$\Delta\tilde{G}^{(N)} = m_N X^{(N)}, \tag{2.15}$$

where we have defined

$$X^{(N)} \equiv \left(\sum_{q=u,d,s}\frac{1}{m_q}\right)^{-1}\left[\left(\sum_{q=u,d,s}\frac{\Delta q^{(N)}}{m_q}\right) - \frac{\eta}{m_N}\right]. \tag{2.16}$$

As we see in Eq. (2.15), the natural scale of the pseudoscalar $\Delta\tilde{q}^{(N)}$ coefficients is greater than the natural scale of the axial-vector $\Delta q^{(N)}$ coefficients by a factor of m_N/m_q. This effect thus tends to *enhance* the pseudoscalar couplings relative to the axial-vector couplings, thereby giving us hope that we might eventually be able to overcome the velocity suppression that afflicts the case of pseudoscalar scattering.

It is perhaps worth pausing to discuss the theoretical origin of this enhancement factor. In general, the definition of the $\Delta q^{(N)}$ coefficients in Eq. (2.3) suggests that these coefficients are fractional quantities which describe "how much" of some physical quantity associated with the nucleon N can be attributed to a constituent quark q. For example, in the case of the axial-vector coefficients, this physical quantity is spin, and the corresponding $\Delta q^{(N)}$ coefficient is known as a spin fraction. Naïvely, this would lead one to expect that the quantities $\Delta q^{(N)}$ should be relatively small, and certainly less than one. However, there is also another feature whose effects are reflected in the magnitudes of these coefficients: this is the difference in the intrinsic overall normalizations associated with the quark and nucleon fields q and N respectively. Indeed, as is conventional, each field q or N is normalized to its mass so that the corresponding state kets will satisfy relations such as $\langle q|q\rangle = 2m_q$ and $\langle N|N\rangle = 2m_N$ [or, equivalently, relations such as those in Eq. (2.6)]. Thus, quantities such as the $\Delta q^{(N)}$ coefficients which convert from quark currents to nucleon currents will also intrinsically include factors that reflect this change in normalization.

Given this, it might be tempting to identify the pseudoscalar enhancement factor m_N/m_q appearing in Eq. (2.15) as reflecting this second contribution, namely a change in normalization. However, we can easily see that this is *not* the case: the axial-vector coefficients $\Delta q^{(N)}$ and the pseudoscalar coefficients $\Delta\tilde{q}^{(N)}$ each already intrinsically incorporate such normalization factors, yet our enhancement factor in Eq. (2.15) is one which rescales our pseudoscalar coefficients *relative to the axial-vector coefficients.* Indeed, this is an *extra* enhancement which emerges *beyond* the mere effects of normalization, and which ultimately reflects the fact that the pseudoscalar and axial-vector coefficients are locked together as a single degree of freedom through a relation such as that in Eq. (2.10). Or, phrased somewhat differently, the factor of $2m_\psi$ which appears in Eq. (2.10)—and which ultimately leads directly to our enhancement factor in Eq. (2.15), thereby driving the $\Delta\tilde{q}^{(N)}$ coefficients above unity—follows not from a normalization but rather from an *equation of motion*. Thus, our enhancement factor reflects far more than mere normalization conversion; it is instead deeply rooted in the dynamics of the quark and nucleon fields and the fact that their corresponding pseudoscalar and axial-vector currents are tied together through Eq. (2.10).

Using the algebraic results in Eq. (2.15) and the numerical results in Table I, we can evaluate the $\Delta\tilde{q}^{(N)}$ coefficients explicitly. Our results, along with associated uncertainties, are shown in Table II. As we see, the pseudoscalar $\Delta\tilde{q}^{(N)}$ coefficients are indeed larger than the corresponding axial-vector $\Delta q^{(N)}$ coefficients in Table I by a factor of $\mathcal{O}(10^2$–$10^3)$ in each case, as promised. Indeed, as we shall demonstrate below, it is precisely the relatively large size of the pseudoscalar coefficients $\Delta\tilde{q}^{(N)}$ which compensates for the velocity suppression. For these numerical calculations, we have taken $\eta = 0.0 \pm 0.33$, as discussed above, and we have taken the masses of the light quarks (and their associated uncertainties) from Ref. [26]. In particular, we have taken $m_u = 2.3 \pm 0.7$ MeV, $m_d = 4.8 \pm 0.5$ MeV,

TABLE II. Numerical values for the pseudoscalar coefficients $\Delta\tilde{q}^{(N)}$, as obtained from Eq. (2.15). Details concerning the calculation of these quantities and their associated uncertainties are discussed in the text. It is readily observed that these pseudoscalar coefficients $\Delta\tilde{q}^{(N)}$ are larger than the corresponding axial-vector coefficients $\Delta q^{(N)}$ in Table I by a factor of $\mathcal{O}(10^2$–$10^3)$. This can enhance the dark-matter/nucleon scattering amplitudes associated with pseudoscalar interactions, and thereby potentially overcome the velocity suppression that would otherwise render such cases unobservable in direct-detection experiments.

	$N = p$	$N = n$
$\Delta\tilde{u}^{(N)}$	110.55 ± 21.87	-108.03 ± 21.33
$\Delta\tilde{d}^{(N)}$	-107.17 ± 21.14	108.60 ± 21.29
$\Delta\tilde{s}^{(N)}$	-3.37 ± 1.01	-0.57 ± 0.78
$\Delta\tilde{G}^{(N)}$	(395.2 ± 124.4) MeV	(35.7 ± 95.4) MeV

and $m_s = 95 \pm 5$ MeV, corresponding to the quark masses at the renormalization scale $\mu = 2$ GeV in the $\overline{\text{MS}}$ renormalization scheme, and then rescaled each mass and uncertainty by a factor of 1.35 in order to account for the effect of renormalization-group running down to the scale $\mu \approx 1$ GeV appropriate for dark-matter/nucleon scattering [26]. All uncertainties were then added together in quadrature in order to produce the final uncertainties quoted in Table II.

As evident from Table II, the results for the pseudoscalar $\Delta\tilde{q}^{(N)}$ coefficients no longer respect quark-level isospin invariance, as defined in Eq. (2.8). [In this connection we observe that quark-level isospin invariance would also require $\Delta\tilde{G}^{(p)} = \Delta\tilde{G}^{(n)}$.] This is a clear distinction relative to the axial-vector case in Table I, but there are several ways in which to understand this result. At an algebraic level, the breaking of quark-level isospin invariance arises because the transition from the axial-vector coefficients to the pseudoscalar coefficients explicitly involves the quark masses; by contrast, the axial-vector coefficients were derived under approximations in which the light quarks are effectively treated as massless. Or, phrased somewhat differently, the leading terms in the axial-vector matrix elements are independent of the quark masses; it is only the subleading terms which depend on these masses explicitly. This is different from the situation one faces in dealing with the pseudoscalar matrix elements, for which the leading terms are already mass dependent. On a more physical level, this difference can alternatively be understood as arising from the fact that the axial-vector current is somewhat special in that its matrix element essentially counts the number of fermions minus antifermions, weighted by chirality and normalized to the mass of the nucleon bound state. [This is analogous to the vector-current matrix element, which also counts the normalized number of fermions minus antifermions but without a chirality weighting.] As a result, the leading-order results in the axial-vector case depend on the number and charges of the parton constituents, but not their masses. This is to be contrasted with the pseudoscalar matrix elements, for which an additional quark mass dependence can arise.

It should also be noted that while the uncertainties quoted in Table II are reliable in terms of their approximate overall magnitudes, there are certain effects which we have not taken into account which might alter these results slightly. Such effects will be discussed more fully as part of an exhaustive uncertainty analysis in Ref. [27]. For example, we have treated the uncertainties in Table I for the axial-vector $\Delta q^{(N)}$ coefficients as independent of each other (i.e., uncorrelated), but in truth (see, e.g., Ref. [8]) the $\Delta u^{(N)}$ and $\Delta d^{(N)}$ coefficients are actually extracted as linear combinations of two more fundamental variables $a_3^{(N)}$ and $a_8^{(N)}$. It is actually the uncertainties on these latter variables which are independent, not those on the $\Delta q^{(N)}$ coefficients. Likewise, the uncertainties on the quark masses are also not independent, as these masses are typically extracted in terms of a single reference quark mass (typically that of the down quark) and the ratios of the other quark masses relative to this reference mass. The truly independent uncertainties are therefore those for the down-quark mass and the corresponding ratios. Moreover, the uncertainties on the quark masses are not necessarily Gaussian, since they typically have both systematic and random contributions. Combining these into a single uncertainty, as we have done here, and then treating this single uncertainty as Gaussian when performing a quadrature-based analysis represents yet another approximation. Indeed, η is an example of a variable whose uncertainty is completely systematic rather than experimental, yet its uncertainty is being treated as if it were Gaussian as well. Finally, there is even some leeway concerning how one treats isospin symmetry in a rigorous uncertainty analysis. Isospin symmetry, as mentioned above, is usually invoked in order to relate quantities such as $\Delta u^{(p)}$ and $\Delta d^{(n)}$—indeed, it is typically the case that these quantities are not measured independently. As a result of this presumed isospin symmetry, these quantities are necessarily quoted as having the same central values and same quoted uncertainties, as indicated in Table I. However, it is not clear whether these uncertainties should be treated as independent or correlated when performing a quadrature-based uncertainty analysis of the sort we are performing here. While isospin symmetry would dictate that these uncertainties be treated as completely correlated, we know that isospin symmetry is only approximate in nature. Indeed, as mentioned above, the results in Table II for the central values of our pseudoscalar $\Delta\tilde{q}^{(N)}$ coefficients already fail to respect isospin symmetry because of their explicit dependence on the light-quark masses. We have therefore opted to treat the uncertainties in Table I as completely independent and uncorrelated.

Despite these observations, the uncertainties quoted in Table II are correct in terms of their overall magnitudes. It is also evident that the pseudoscalar uncertainties quoted in

Table II are somewhat larger, in relative terms, than the corresponding axial-vector uncertainties quoted in Table I. This is partially due to the dependence of the pseudoscalar results on a constraint which stems from a large-N_c approximation. As a result of these larger uncertainties, we see that certain quantities in Table II, such as $\Delta\tilde{s}^{(n)}$ and $\Delta\tilde{G}^{(n)}$, are actually consistent with zero. As we shall see, these results will lead to considerably larger uncertainties for our eventual pseudoscalar dark-matter/nucleon couplings.

Finally, we now turn to the pseudoscalar $\Delta\tilde{q}^{(N)}$ coefficients for the heavy quarks $q = Q \equiv c, b, t$. As we shall see, these quantities will be relevant if our dark matter couples to such quarks. In the axial-vector case, the analogous coefficients were taken to be zero, reflecting the fact that such quarks are heavy and make only negligible contributions to axial-vector couplings. For pseudoscalar couplings, by contrast, the situation is different. Because of the current-algebra relation in Eq. (2.10), we see that the pseudoscalar current is related to the *derivative* of a different current involving the same heavy fermions. However, if the fermions in question are sufficiently heavy, they will have no dynamics and this derivative must vanish. We thus obtain the relation

$$2m_Q\langle N_f|\bar{Q}i\gamma^5 Q|N_i\rangle = -\frac{\alpha_s}{4\pi}\langle N_f|G\tilde{G}|N_i\rangle, \tag{2.17}$$

from which we see that

$$\begin{aligned}\langle N_f|\bar{Q}i\gamma^5 Q|N_i\rangle &= -\frac{1}{m_Q}\frac{\alpha_s}{8\pi}\langle N_f|G\tilde{G}|N_i\rangle \\ &= -\frac{1}{m_Q}\Delta\tilde{G}^{(N)}\langle N_f|\bar{N}i\gamma^5 N|N_i\rangle,\end{aligned} \tag{2.18}$$

where the values of $\Delta\tilde{G}^{(N)}$ are given algebraically in Eq. (2.15). We thus find that

$$\Delta\tilde{Q}^{(N)} = -\frac{1}{m_Q}\Delta\tilde{G}^{(N)}. \tag{2.19}$$

C. Pseudoscalar dark-matter/nucleon couplings and the effects of isospin violation

We now turn to the actual quantities $g_{\chi N}$ which parametrize how the dark-matter fermion χ couples to nucleons N in the case of pseudoscalar interactions. As evident in Eq. (2.5), these effective couplings $g_{\chi N}$ are directly determined in terms of the $\Delta\tilde{q}^{(N)}$ coefficients for both light and heavy quarks:

$$g_{\chi N} = \sum_{q=u,d,s} c_q\Delta\tilde{q}^{(N)} - \sum_{Q=c,b,t}\frac{c_Q}{m_Q}\Delta\tilde{G}^{(N)}, \tag{2.20}$$

where the numerical values of the $\Delta\tilde{q}^{(N)}$ and $\Delta\tilde{G}^{(N)}$ coefficients are listed in Table II.

The only task remaining, then, is to determine the values for the quark couplings c_q (henceforth taken to collectively denote the couplings for both light and heavy quarks). Of course, the expression in Eq. (2.20) for the $g_{\chi N}$ is completely general and applicable for any choice of operator coefficients c_q in the fundamental theory. In principle, any assignment of the c_q consistent with phenomenological constraints is therefore permitted. However, for concreteness, in this paper we shall focus primarily on three particular benchmark scenarios:

- *Scenario I.*—The case in which the c_q for all up-type quarks take a common value $c_u = c_c = c_t$ and the c_q for all down-type quarks likewise take a (potentially different) common value $c_d = c_s = c_b$. For this scenario, we parametrize these two independent operator coefficients in terms of a mass scale $M_{\rm I}$ and an angle θ such that $c_u/\Lambda^2 = \cos\theta/M_{\rm I}^2$ and $c_d/\Lambda^2 = \sin\theta/M_{\rm I}^2$. It then follows that $\tan\theta = c_d/c_u$ and $M_{\rm I}^2 = \Lambda^2/\sqrt{c_u^2 + c_d^2}$. Note that for $\theta = \pi/4$, this coupling structure respects quark-level isospin invariance. Varying θ will thus allow us to study the effects of isospin violation in a continuous fashion.
- *Scenario II.*—A generalization of the oft-studied case in which the c_q are proportional to the Yukawa couplings y_q between the quarks and the SM Higgs boson, and thus to m_q. This scenario is motivated by the minimal-flavor-violation assumption that the quark Yukawa couplings are wholly responsible for flavor violations. The generalization we consider here is one in which the c_q for the up-type quarks may also be scaled by an overall multiplicative factor relative to the c_q for the down-type quarks. Specifically, for this scenario, we define a mass scale $M_{\rm II}$ and an angle θ such that $c_q/\Lambda^2 = m_q\cos\theta/M_{\rm II}^3$ for up-type quarks and $c_q/\Lambda^2 = m_q\sin\theta/M_{\rm II}^3$ for down-type quarks. It then follows that $\tan\theta = (c_d m_u)/(c_u m_d)$ and $M_{\rm II}^3 = \Lambda^2/\sqrt{(c_u/m_u)^2 + (c_d/m_d)^2}$, where $c_u/m_u = c_c/m_c = c_t/m_t$ and $c_d/m_d = c_s/m_s = c_b/m_b$.
- *Scenario III.*—The related case in which the c_q are nonvanishing only for the first-generation quarks—i.e., in which c_u and c_d are arbitrary, but in which $c_s = c_c = c_b = c_t = 0$. For this scenario, we likewise define $M_{\rm III}$ and θ such that $c_u/\Lambda^2 = m_u\cos\theta/M_{\rm III}^3$ and $c_d/\Lambda^2 = m_d\sin\theta/M_{\rm III}^3$. This coupling structure is of particular interest from a direct-detection perspective, implying that c_u and c_d uniquely determine the effective dark-matter/nucleon couplings $g_{\chi p}$ and $g_{\chi n}$ in Eq. (2.21), and vice versa. Moreover, with the couplings for the second- and third-generation quarks set to zero, this scenario is the only one which does not involve couplings which are essentially irrelevant for direct detection. Since nonzero couplings for second- and third-generation quarks could potentially have a significant effect on the rates for dark-matter production at colliders [28], this scenario is therefore in some sense the most

"conservative" in that it does not assume any channels which might enhance collider signatures without affecting direct-detection signals. Study of this scenario will therefore lead to the most conservative set of limits consistent with collider data.

We emphasize that these three scenarios represent physically distinct coupling structures between χ and the SM quarks. It is for this reason that each scenario has been associated with its own independent mass scale above.

Given these three scenarios, we can now proceed to examine the behavior of our pseudoscalar dark-matter/nucleon couplings as functions of θ in each scenario. For Scenario I, the results in Table II yield the effective pseudoscalar couplings

$$g_{\chi p} = 110.2\cos\theta - 110.6\sin\theta,$$
$$g_{\chi n} = -108.1\cos\theta + 108.0\sin\theta. \tag{2.21}$$

Likewise, given the uncertainties in Table II, we find that the associated *uncertainties* in these couplings are given by rather complicated expressions which can be extremely well approximated as

$$\delta g_{\chi p} \approx |21.79\cos\theta - 21.88\sin\theta|,$$
$$\delta g_{\chi n} \approx |21.32\cos\theta - 21.33\sin\theta|. \tag{2.22}$$

We immediately note that both the couplings *and* their associated uncertainties are nearly vanishing at the quark-level isospin-preserving point $\theta = \pi/4$. Alternatively, given the couplings in Eq. (2.21), we can solve for the value θ^* at which *nucleon-level* isospin preservation takes place—i.e., the value θ^* at which $g_{\chi p} = g_{\chi n}$. We find that in this scenario, the nucleon-level isospin-preserving point is extremely close to the quark-level isospin-preserving point, with only a very small net displacement $\theta^* - \pi/4 \approx -8.45 \times 10^{-4}$ radians.

At the nucleon-level isospin-preserving point, we find that $g_{\chi p} = g_{\chi n} \approx -0.155 \pm 0.25$—a value consistent with zero. This is remarkable, representing a situation in which dark matter couples to quarks, but not to nucleons! Moreover, this is to be compared with the couplings that emerge for other, isospin-violating values of θ. For example, we find that the proton coupling takes the value $|g_{\chi p}| \approx 110.6 \pm 21.9$ at $\theta = \pi/2$, and reaches a maximum value $|g_{\chi p}| \approx 156.2 \pm 30.9$ at $\theta \approx 3\pi/4$. The behavior of the neutron coupling $|g_{\chi n}|$ is similar. Thus, relative to the central values of these couplings at the isospin-preserving point $\theta = \theta^*$, we see that these couplings experience a huge enhancement which can grow as large as a factor of 10^3!

It is important to understand the physical origin of the cancellation of this coupling in the isospin-preserving case. Ultimately, this cancellation is the direct result of the fact that we (like most researchers in this field) are working in the large-N_c chiral limit in which relations such as that in Eq. (2.12) apply. Indeed, since the strange-quark contribution in Eq. (2.12) is small, this relation immediately implies that the isospin-conserving case will experience a cancellation. At a physical level, this can equivalently be understood as follows. In general, one can consider an approximation in which dark-matter/nucleon scattering is considered to be mediated by neutral-meson exchange. In this approximation, the dominant contribution is from pion exchange, and the pion couples to the first-generation quarks in a way which is maximally isospin-violating. (By contrast, the *isospin-conserving* case would involve the η and η' states as mediators, but these states are much heavier than the pion.) Indeed, Eq. (2.12) emerges in the large-N_c chiral limit precisely because this is the limit in which the η' decouples. Nevertheless, we have also explicitly taken into account possible small departures from the large-N_c limit when we introduce our η-dependent "error" term in Eq. (2.13). The fact that the proton and neutron couplings continue to vanish—even within the resulting uncertainties—demonstrates that this cancellation is robust against small departures from the large-N_c limit.

We therefore conclude that isospin violation in Scenario I produces a huge enhancement in the corresponding pseudoscalar proton and neutron couplings. This is the direct result of the relatively large pseudoscalar coefficients $\Delta\tilde{q}^{(N)}$ in Table II, operating within the framework of the particular quark coupling structure associated with Scenario I. However, it is important to stress that there is nothing intrinsic to the coupling structure of Scenario I by itself which causes such large proton and nucleon couplings to emerge. For example, as an algebraic exercise, we can calculate the proton and neutron couplings that would emerge under Scenario I in the *axial-vector* case—i.e., using the axial-vector coefficients $\Delta q^{(N)}$ in Table I rather than the pseudoscalar coefficients $\Delta\tilde{q}^{(N)}$ in Table II. In this case, because of the fact that isospin symmetry is exactly preserved for the $\Delta q^{(N)}$ coefficients, both quark-level and nucleon-level isospin preservation coincide exactly at $\theta = \pi/4$. Indeed, at this point we find $g_{\chi p} = g_{\chi n} \approx 0.303 \pm 0.12$, while the maximum value taken by these couplings for any isospin-violating value of θ is $|g_{\chi p}| \approx 0.865 \pm 0.15$ at $\theta \approx 2.714$ and $g_{\chi n} \approx 0.812 \pm 0.15$ at $\theta \approx 1.974$. Thus, for the axial-vector case, we see that isospin violation is capable of increasing the proton and neutron couplings only by mere factors of 2.85 and 2.68 respectively.

We also note, of course, that the overall *scale* of the axial-vector couplings is significantly smaller than that for the pseudoscalar couplings. While it is perhaps inappropriate to compare the magnitudes of these different couplings against each other (because they correspond to different operators with gamma-matrix bilinears exhibiting entirely different tensorial properties), at a purely algebraic level this difference can once again be attributed to the larger values of the $\Delta\tilde{q}^{(N)}$ coefficients that enter the

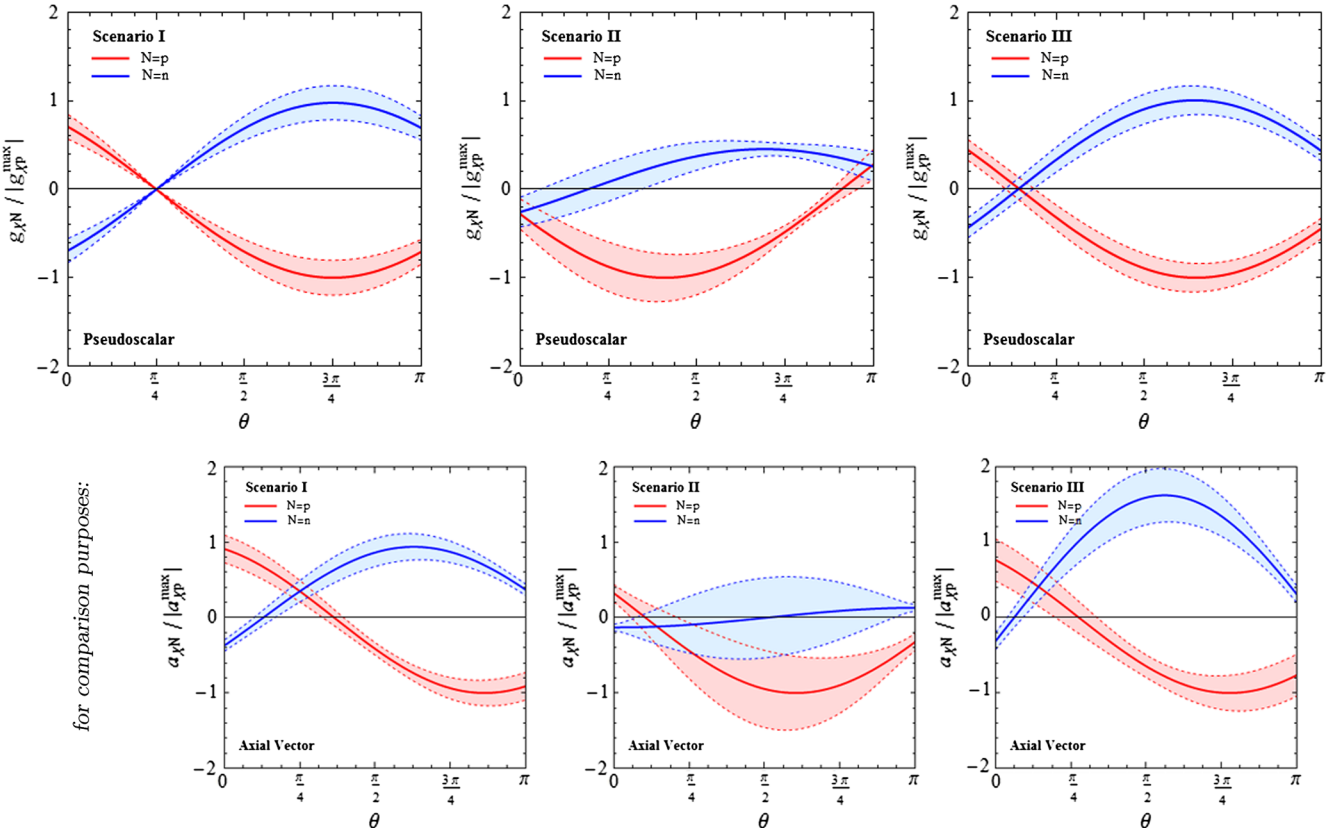

FIG. 1 (color online). The effective proton and neutron dark-matter couplings $g_{\chi p}$ (red) and $g_{\chi n}$ (blue), plotted as functions of θ for each of the three coupling scenarios discussed in the text. Panels in the upper row show the behavior of the pseudoscalar couplings in each scenario, while the panels in the lower row show the behavior of the corresponding axial-vector couplings. The dashed lines in each panel correspond to the central values for these couplings, while the shaded regions indicate the 1σ uncertainty bands around these central values. Note that in each panel, both $g_{\chi p}$ and $g_{\chi n}$ have been normalized to the maximum possible central value of $|g_{\chi p}|$ attainable in each scenario.

calculation of the pseudoscalar proton and neutron couplings as compared with the values of the $\Delta q^{(N)}$ coefficients that enter the calculation of their axial-vector counterparts.

In Fig. 1, we have plotted the pseudoscalar proton and neutron couplings $g_{\chi p}$ and $g_{\chi n}$, along with their corresponding uncertainties, as functions of θ for all three of our coupling scenarios. For comparison purposes, we have also plotted the corresponding axial-vector couplings as functions of the same variable θ. Moreover, in each case we have normalized the proton and neutron couplings to the maximum value that the proton coupling ever attains as a function of θ.

Many features of these plots are worthy of note. Focusing first on the pseudoscalar couplings, we have already remarked that a significant degree of cancellation occurs within Scenario I when isospin is conserved at the nucleon level: both the proton and neutron pseudoscalar couplings, along with their associated uncertainties, become extremely small as a result of a near-perfect cancellation between their individual up-quark and down-quark contributions. As remarked earlier, this is then a situation in which our dark matter couples to quarks, but not to nucleons! What is now apparent from Fig. 1, however, is that this cancellation is a relatively sharp one, and that any movement away from this isospin-conserving value of θ in either direction results in a significant enhancement of these pseudoscalar nucleon couplings. As indicated above, this results in an $\mathcal{O}(10^3)$ enhancement in the pseudoscalar couplings for isospin-violating scenarios relative to the naïve isospin-conserving case, and thus to an $\mathcal{O}(10^6)$ enhancement in the cross section for the scattering of χ off atomic nuclei. Thus, we see that even a relatively small amount of isospin violation can have a dramatic effect on direct-detection rates!

The above behavior occurs for Scenario I. However, we now see from Fig. 1 that similar behavior also occurs for Scenario III, albeit at a somewhat shifted value of θ. This feature is also easy to understand. In Scenario I, the cancellation that occurs at θ^* truly reflects an approximate isospin symmetry. Indeed, while the term in Eq. (2.20) proportional to $\Delta\tilde{G}^{(N)}$ is manifestly isospin-violating, this contribution is suppressed by several orders of magnitude compared to the contributions from the light quarks in this

scenario. Moreover, since the c_q are independent of the quark masses in Scenario I and since the $\Delta\tilde{q}^{(N)}$ are *approximately* isospin-conserving (particularly for the two lightest quarks), this cancellation occurs for a value of θ^* very close to $\theta \approx \pi/4$. Of course, in Scenario III, the $\Delta\tilde{G}^{(N)}$ contribution to the couplings vanishes outright because the dark-matter particle does not couple to the heavy quarks. However, the above cancellation now occurs at the value $\theta^* = \tan^{-1}(m_u/m_d) \approx 0.45$ rather than at $\theta^* \approx \pi/4$, for within Scenario III it is only at this shifted angle that $c_u = c_d$. Furthermore, within Scenario III, we see that the uncertainties are no smaller at θ^* than they are at any other angle—another distinction relative to Scenario I.

Finally, we observe that the pseudoscalar couplings shown for Scenario II differ quite significantly from those shown for Scenario III, both in terms of the locations of the nucleon-level isospin-preserving points as well as the overall magnitudes of the associated uncertainties. These differences ultimately reflect the contributions from the second- and third-generation quarks. One notable feature in Scenario II, for example, is the fact that the sort of cancellation which occurs for Scenarios I and III does not occur for Scenario II. The reason for this is also easy to understand. In Scenario II, we have $c_q \propto m_q$ for all quark species. For such a coupling structure, it turns out that the magnitudes of the two terms on the right side of Eq. (2.20) are roughly commensurate. Thus, even if θ were set at a value for which the light-quark contributions roughly canceled, the heavy-quark contributions would still be significant. Indeed, for this scenario, we find that nucleon-level isospin preservation arises at $\theta^* \approx 3.12$—a value much closer to π than to $\pi/4$—but the proton and neutron couplings at this point are clearly nonzero.

In Fig. 1 we have also illustrated what occurs for the corresponding *axial-vector* couplings in each scenario. For example, as already discussed above, we see that the isospin-preserving points no longer correspond to vanishing proton and neutron couplings—even for Scenarios I and III. Thus isospin violation will no longer produce as dramatic an enhancement for the axial-vector proton and neutron couplings as it does for the corresponding pseudoscalar couplings, even in these scenarios. Moreover, we observe that unlike the situation for the pseudoscalar couplings, there are no values of θ in Scenarios I or III for which both $g_{\chi p}$ and $g_{\chi n}$ vanish simultaneously. Thus, for axial-vector couplings, dark-matter couplings to quarks always imply a dark-matter coupling to at least one nucleon. Furthermore, we see that the uncertainties are so large for the axial-vector neutron coupling in Scenario II that the value of this coupling is consistent with zero for almost all values of θ. Finally, although it is not visible from the plots in Fig. 1, we again stress that the overall magnitude of the axial-vector couplings is a factor of $\mathcal{O}(10^2$–$10^3)$ smaller than the magnitude of the pseudoscalar couplings. This is perhaps the most important difference of all.

Despite the rather compelling nature of these differences, it is important to bear in mind that the pseudoscalar and axial-vector couplings correspond to entirely different operators. Thus, a direct comparison between these couplings is fraught with a number of theoretical subtleties. For example, Scenarios II and III are rather unnatural within an axial-vector framework, and it is difficult to imagine a high-scale model which might yield such an axial-vector effective operator with the quark-level couplings of Scenarios II or III at lower energies. This is completely different from what happens within the pseudoscalar framework, where the coupling structures of Scenarios II and III are particularly well motivated. Nevertheless, we have undertaken such a direct coupling-to-coupling comparison in order to expose the primary numerical differences that emerge when the axial-vector $\Delta q^{(N)}$ coefficients of Table I are replaced with the pseudoscalar $\Delta\tilde{q}^{(N)}$ coefficients of Table II. Indeed, from a purely bottom-up perspective, the coupling structures of all three scenarios can be taken to represent interesting benchmarks which are introduced purely for the purpose of studying varying resulting phenomenologies in a model-independent framework. We have therefore chosen to study the resulting couplings free of any theoretical prejudice stemming from considerations of high-scale physics.

Of course, what ultimately matters in each case are not the couplings themselves, but rather the implications of these couplings for the reach of actual direct-detection experiments. For example, we have seen that even a small amount of isospin violation can dramatically enhance our pseudoscalar couplings, but it remains to be seen whether this effect is large enough to compensate for the velocity suppression which is also associated with pseudoscalar interactions, and thereby render such interactions potentially relevant for detection at the next generation of spin-dependent dark-matter direct-detection experiments. This is therefore the topic to which we now turn.

III. *CP* OR NOT *CP*, THAT IS THE QUESTION: AN INTERLUDE ON THE CHOICE OF LAGRANGIAN OPERATORS

In this paper, our analysis has focused on those interactions between dark matter and Standard-Model matter which take the form of effective four-Fermi contact interactions whose operators exhibit the double-bilinear form in Eq. (2.1). Thus far, our interest has focused on the unique physics that emerges from assuming a pseudoscalar structure for the quark bilinear in Eq. (2.1), and indeed all of our results thus far have relied on this choice. However, we have yet to select a tensor structure for the corresponding dark-matter bilinear, and Lorentz invariance dictates that there are only two possible choices open to us:

$$\mathcal{O}_{\chi q}^{(\mathrm{SP})} \equiv \frac{c_q}{\Lambda^2}(\bar{\chi}\chi)(\bar{q}i\gamma^5 q),$$
$$\mathcal{O}_{\chi q}^{(\mathrm{PP})} \equiv \frac{c_q}{\Lambda^2}(\bar{\chi}i\gamma^5\chi)(\bar{q}i\gamma^5 q). \quad (3.1)$$

The first of these operators breaks CP symmetry, while the second preserves it. Unfortunately, we can proceed no further in our discussion of actual direct-detection experimental prospects without making a specific choice between these two operators.

The CP-violating operator $\mathcal{O}_{\chi q}^{(\mathrm{SP})}$ is often neglected in direct-detection studies, even in comparison with $\mathcal{O}_{\chi q}^{(\mathrm{PP})}$. One reason for this is that $\mathcal{O}_{\chi q}^{(\mathrm{PP})}$ is CP invariant and can therefore be generated at a nontrivial level in many top-down theoretical constructions which yield a stable dark-matter candidate, such as the constrained minimal supersymmetric model (CMSSM) in which there is no additional source of CP violation. However, in a bottom-up effective-theory approach such as the one we adopt here, the aim is to examine and constrain the properties of all possible interactions which could arise between the dark-matter candidate and the particles of the SM in as model-independent a framework as possible, without theoretical prejudice. Indeed, while the operator $\mathcal{O}_{\chi q}^{(\mathrm{PP})}$ is typically assumed to be irrelevant for direct detection, it is instructive to revisit why this is the case—and also why this is *not* the case for $\mathcal{O}_{\chi q}^{(\mathrm{SP})}$, despite the fact that the structure of the quark bilinear is the same in both cases.

Let us first consider the situation in which χ couples to SM particles primarily via $\mathcal{O}_{\chi q}^{(\mathrm{PP})}$. We assume for the purposes of this discussion that this operator provides the dominant contribution both to the cross section for nuclear scattering events at direct-detection experiments and to the annihilation rate of χ and $\bar{\chi}$ in the early universe. For purposes of illustration, we also restrict our attention to the case in which χ couples to only one quark flavor; thus only one of the c_q is nonvanishing. We have already seen for $\mathcal{O}_{\chi q}^{(\mathrm{PP})}$ that both the dark-matter bilinear and the quark bilinear give rise to a velocity suppression in the dark-matter/nucleon cross section for direct detection. Thus, for $\mathcal{O}_{\chi q}^{(\mathrm{PP})}$, the resulting (spin-dependent) cross section can be expected to scale like

$$\mathrm{PP}: \quad \sigma_{\mathrm{SD}}^{(\chi N)} \sim \frac{c_q^2[\Delta\tilde{q}^{(N)}]^2\mu_{\chi N}^6 v^4}{m_\chi^2 m_N^2 \Lambda^4}, \quad (3.2)$$

where $\mu_{\chi N} \equiv m_\chi m_N/(m_\chi + m_N)$ denotes the reduced mass of the χ/nucleon system.

There are clearly many unknown parameters in Eq. (3.2), making it difficult to provide an actual numerical estimate of this cross section. However, we may appeal to a somewhat orthogonal constraint which applies to any thermal dark-matter candidate: that through which the annihilation rate of χ and $\bar{\chi}$ sets an overall dark-matter abundance in the early universe. For $\mathcal{O}_{\chi q}^{(\mathrm{PP})}$, the annihilation of χ and $\bar{\chi}$ in the early universe has no chirality suppression since the initial state is CP odd, with quantum numbers $S = 0, L = 0$, and $J = 0$ [15]. In an s-wave annihilation scenario of this sort, the thermal annihilation cross section $\langle\sigma|v|\rangle$ scales like

$$\mathrm{PP}: \quad \langle\sigma|v|\rangle \sim \frac{c_q^2 m_\chi^2}{\Lambda^4} \quad (3.3)$$

at around the time of freeze-out. Moreover, in order for the relic-abundance contribution from freeze-out to agree with observation (i.e., $\Omega_\chi \approx \Omega_{\mathrm{DM}}$), this cross section must be roughly $\langle\sigma|v|\rangle \sim 1$ pb at such times.

Given this constraint, we can substitute back into Eq. (3.2) in order to find that

$$\mathrm{PP}: \quad \sigma_{\mathrm{SD}}^{(\chi N)} \sim (1\ \mathrm{pb}) \times \frac{[\Delta\tilde{q}^{(N)}]^2\mu_{\chi N}^6 v^4}{m_\chi^4 m_N^2}. \quad (3.4)$$

Since $v^4 \sim \mathcal{O}(10^{-12})$, we see that extremely large values of $\Delta\tilde{q}^{(N)}$ would be required to overcome this velocity suppression and yield a χ/nucleon cross section of sufficient magnitude to be probed at any foreseeable direct-detection experiment, even for low-mass dark matter. Indeed, since both $\langle\sigma|v|\rangle$ and $\sigma_{\mathrm{SD}}^{(\chi N)}$ depend on Λ in the same manner for a thermal relic, this unhappy consequence exists regardless of the scale Λ at which Ω_χ is generated via thermal freeze-out for a dark-matter particle with this coupling structure. Unfortunately, we have already seen that our pseudoscalar $\Delta\tilde{q}^{(N)}$ coefficients, although significantly enhanced relative to their axial-vector counterparts, are not large enough to overcome this degree of velocity suppression. Thus we do not expect the operator $\mathcal{O}_{\chi q}^{(\mathrm{PP})}$ to have much relevance for direct-detection experiments.

Let us now turn to the situation in which χ primarily couples to SM particles through the operator $\mathcal{O}_{\chi q}^{(\mathrm{SP})}$. In sharp contrast to the $\mathcal{O}_{\chi q}^{(\mathrm{PP})}$ case discussed above, in this case only the quark bilinear gives rise to a velocity suppression in the cross section for nonrelativistic χ/nucleon scattering. This cross section therefore scales like

$$\mathrm{SP}: \quad \sigma_{\mathrm{SD}}^{(\chi N)} \sim \frac{c_q^2[\Delta\tilde{q}^{(N)}]^2\mu_{\chi N}^4 v^2}{m_N^2 \Lambda^4}. \quad (3.5)$$

Moreover, in this case we see that dark-matter annihilation in the early universe is p-wave suppressed, since the initial state is CP even, with quantum numbers $S = 1, L = 1$, and $J = 0$. The annihilation cross section in this case scales like

$$\mathrm{SP}: \quad \langle\sigma|v|\rangle \sim v_{\chi,\mathrm{fr}}^2 \frac{c_q^2 m_\chi^2}{\Lambda^4}, \quad (3.6)$$

where $v_{\chi,\mathrm{fr}}$ denotes the average speed of χ and $\bar{\chi}$ at freeze-out. Typically, $v_{\chi,\mathrm{fr}}^2 \sim 0.1$. Imposing, as before, the condition $\langle\sigma|v|\rangle \sim 1$ pb in order to ensure that $\Omega_\chi \approx \Omega_{\mathrm{DM}}$, we find that

$$\text{SP:}\quad \sigma_{\text{SD}}^{(\chi N)} \sim (1\ \text{pb}) \times \frac{10[\Delta\tilde{q}^{(N)}]^2 \mu_{\chi N}^4 v^2}{m_\chi^2 m_N^2}. \tag{3.7}$$

Since the velocity suppression $v^2 \sim \mathcal{O}(10^{-6})$ obtained in this case is far less severe than that obtained in Eq. (3.4), we see that only moderately large values for the $\Delta\tilde{q}^{(N)}$ coefficients are required in order to compensate for this velocity suppression and render the operator $\mathcal{O}_{\chi q}^{(\text{SP})}$ relevant for direct detection. Moreover, as we have seen in Sec. II, these coefficients are indeed enhanced by the required amount.

We thus conclude that $\mathcal{O}_{\chi q}^{(\text{SP})}$, rather than $\mathcal{O}_{\chi q}^{(\text{PP})}$, has greater prospects for being relevant to future direct-detection experiments. As a result, we shall concentrate on $\mathcal{O}_{\chi q}^{(\text{SP})}$ in the remainder of this paper.

IV. PHENOMENOLOGICAL CONSEQUENCES: DIRECT DETECTION AND RELATED BENCHMARKS

We now turn to investigate the direct-detection prospects for a dark-matter candidate in each of the three benchmark coupling scenarios defined in Sec. II C. In particular, we wish to determine the bounds imposed by existing direct-detection data on the corresponding suppression scale M_{I}, M_{II}, or M_{III} in each of these scenarios as a function of the dark-matter mass m_χ and the coupling angle θ, and to assess the extent to which the next generation of direct-detection experiments will be able to probe the remaining parameter space in each scenario.

In interpreting the results of such a direct-detection analysis, it is also useful to examine the relationship between the region of parameter space accessible by direct-detection experiments in each of these coupling scenarios and regions of parameter space which are relevant for other aspects of dark-matter phenomenology. For example, thermal freeze-out offers a natural mechanism for generating a relic abundance of the observed magnitude for a massive dark-matter particle which can annihilate to SM particles. It is therefore interesting to examine whether successful thermal freeze-out can be realized within the region of parameter space accessible to the next generation of direct-detection experiments for a dark-matter particle which annihilates primarily via $\mathcal{O}_{\chi q}^{(\text{SP})}$. In addition, new-physics searches in a variety of channels at the LHC constrain the parameter space of operators which couple the dark and visible sectors. It is therefore also interesting to examine the interplay between these constraints and those from direct-detection data.

The plan of this section is as follows. We begin by briefly reviewing the physics of direct detection and assessing the extent to which the next generation of direct-detection experiments will be capable of probing the parameter space of each of our benchmark coupling scenarios. We then identify the regions of that parameter space which yield a thermal dark-matter relic abundance of the correct order, and discuss how LHC data serve to constrain that parameter space. As we shall see, the magnitudes of the pseudoscalar $\Delta\tilde{q}^{(N)}$ coefficients have a profound effect on the direct-detection phenomenology of a dark-matter particle which interacts with the visible sector primarily via the $\mathcal{O}_{\chi q}^{(\text{SP})}$ operators.

A. Direct detection

The principal physical quantity probed by direct-detection experiments is the total event rate R for dark-matter scattering off the nuclei in the detector target. For a generic dark-matter model, the expectation value for R at any particular such experiment is obtained by integrating the differential rate dR/dE_R over the range of recoil energies E_R probed by that experiment, convolved with the appropriate detector-efficiency function $\mathcal{E}(E_R)$. This differential event rate (for reviews, see, e.g., Refs. [2,4]) is given by the general expression

$$\frac{dR}{dE_R} = \frac{N_T \rho_\chi^{\text{loc}}}{m_\chi} \int_{v>v_{\text{min}}}^{\infty} v f(\vec{v}) \left(\frac{d\sigma_{\chi T}}{dE_R}\right) d^3 v, \tag{4.1}$$

where N_T is the number of nuclei in the detector target, where ρ_χ^{loc} is the local density of χ within the galactic halo, where $f(\vec{v})$ is the velocity distribution of dark-matter particles in the reference frame of the detector, where $v \equiv |\vec{v}|$, and where $d\sigma_{\chi T}/dE_R$ is the differential scattering cross section. The lower limit v_{min} on the integral over halo velocities corresponds to the kinematic threshold for nonrelativistic scattering of a dark-matter particle off one of the target nuclei.

While substantial uncertainties exist concerning many of the aforementioned quantities which characterize the properties of the dark-matter halo, our focus in this paper is on the pseudoscalar nucleon coefficients $\Delta\tilde{q}^{(N)}$ and their implications for direct detection. We therefore adopt a set of standard benchmark assumptions about the dark-matter halo. In particular, we take $\rho_\chi^{\text{loc}} = 0.3\ \text{GeV cm}^{-3}$; we take $f(\vec{v})$ to be Maxwellian, but truncated above the galactic escape velocity $v_{\text{esc}} \approx 550$ km/s in the halo frame; and we take $v_e = 232$ km/s as the speed of the Earth with respect to the dark-matter halo. Moreover, we focus on the case in which χ/nucleus scattering is purely elastic, for which $v_{\text{min}} = \sqrt{E_R m_T / 2\mu_{\chi T}^2}$, where m_T denotes the mass of the target nucleus and where $\mu_{\chi T}$ is the reduced mass of the χ/nucleus system.

The differential cross section for χ/nucleus scattering is given by the general expression

$$\frac{d\sigma_{\chi T}}{dE_R} = \frac{m_T}{2\pi v^2} \langle |\mathcal{M}_{\chi T}|^2 \rangle, \tag{4.2}$$

where $\langle |\mathcal{M}_{\chi T}|^2 \rangle$ is the corresponding squared S-matrix element, averaged over initial spin states and summed over

final spin states. For the scalar-pseudoscalar interaction we are considering here, we recall Eq. (2.7) to find that this matrix element in the nonrelativistic limit takes the form

$$\mathcal{M}_{\chi T} = \sum_{N=n,p} \frac{g_{\chi N}}{\Lambda^2} \langle \chi_f | \bar{\chi}\chi | \chi_i \rangle \langle T_f | \bar{N}\gamma^5 N | T_i \rangle \approx \frac{4 m_\chi m_T}{\Lambda^2} (\xi_\chi^{s'})^\dagger \xi_\chi^s \sum_{N=n,p} \frac{g_{\chi N}}{m_N} \langle T_f | \vec{q} \cdot \vec{S}_N | T_i \rangle, \quad (4.3)$$

where $\langle T_f | \vec{S}_N | T_i \rangle$ denotes the matrix element for the nucleon-spin operator within the target nucleus and where $\vec{q}$ is the momentum transferred to the nucleus. Note that the m_T/m_N factor in Eq. (4.3) arises due to the difference in normalization between the constituent nucleons and the bound-state nucleus, where we have retained the relativistic normalization in both cases. Proceeding by analogy with the axial-vector case [1], we invoke the Wigner-Eckart theorem in order to make the replacement

$$\langle T_f | \vec{S}_N | T_i \rangle \to \frac{\langle S_N \rangle}{J_T} \langle T_f | \vec{J}_T | T_i \rangle \quad (4.4)$$

in Eq. (4.3), where $\langle S_N \rangle / J_T = \langle T_f | S_N | T_i \rangle / J_T$ again represents the fraction of the total nuclear spin carried by the nucleon N. In the approximation that $m_p \approx m_n$, this yields

$$\mathcal{M}_{\chi T} = \frac{4 m_\chi m_T}{J_T \Lambda^2 m_N} (g_{\chi p} \langle S_p \rangle + g_{\chi n} \langle S_n \rangle)(\xi_\chi^{s'})^\dagger \xi_\chi^s \times \langle T_f | \vec{q} \cdot \vec{J}_T | T_i \rangle. \quad (4.5)$$

The spin-averaged squared matrix element is therefore

$$\langle |\mathcal{M}_{\chi T}|^2 \rangle = \frac{16 m_\chi^2 m_T^2}{J_T^2 (2J_T+1) m_N^2 \Lambda^4} (g_{\chi p} \langle S_p \rangle + g_{\chi n} \langle S_n \rangle)^2 \times \sum_{T_i, T_f} \langle T_f | \vec{q} \cdot \vec{J}_T | T_i \rangle \langle T_i | \vec{q} \cdot \vec{J}_T | T_f \rangle = \frac{16 m_\chi^2 m_T^2 |\vec{q}|^2}{3 m_N^2} \frac{J_T+1}{J_T} \left(\frac{g_{\chi p}}{\Lambda^2} \langle S_p \rangle + \frac{g_{\chi n}}{\Lambda^2} \langle S_n \rangle \right)^2. \quad (4.6)$$

Substituting this result into Eq. (4.2) and dividing by $16 m_\chi^2 m_T^2$ in order to account for the difference between relativistic and nonrelativistic normalization conventions for the χ and nucleus states, we arrive at our final expression for the differential cross section for χ/nucleus scattering:

$$\frac{\partial \sigma_{\chi T}^{(\mathrm{SP})}}{\partial E_R} = \frac{m_T^2 E_R}{3\pi v^2 m_N^2} \frac{J_T+1}{J_T} \times \left(\frac{g_{\chi p}}{\Lambda^2} \langle S_p \rangle + \frac{g_{\chi n}}{\Lambda^2} \langle S_n \rangle \right)^2 \tilde{F}^2(E_R), \quad (4.7)$$

where $\tilde{F}^2(E_R)$ is a nuclear form factor. Note that we have explicitly distinguished this form factor from the usual form factor $F^2(E_R) = S(E_R)/S(0)$ associated with spin-dependent scattering via an axial-vector interaction. Indeed, in the axial-vector case, the scattering cross section depends on the projection of $\vec{S}_N$ along the direction of the spin vector $\vec{S}_\chi$ of the dark-matter particle. By contrast, in the scalar-pseudoscalar case, the corresponding cross section depends on the projection of $\vec{S}_N$ along the direction of the momentum transfer [29].

A wealth of data from direct-detection experiments already significantly constrains the set of possible interactions between dark-matter particles and atomic nuclei, and several additional experiments are poised to probe even more deeply over the coming decade into the parameter space of allowed couplings between the dark and visible sectors. For each of our three benchmark coupling scenarios for scalar-pseudoscalar interactions, the relevant parameter space comprises m_χ, θ, and the corresponding suppression scale M_{I}, M_{II}, or M_{III}. The first of these parameters enters the expected event rate for a given detector in a complicated way through the scattering kinematics, while the second and third enter through the ratios $g_{\chi p}/\Lambda^2$ and $g_{\chi n}/\Lambda^2$ in Eq. (4.7), as discussed in Sec. II C.

Since the χ/nucleus interactions which follow from $\mathcal{O}_{\chi q}^{(\mathrm{SP})}$ involve the nuclear spin $\vec{S}_N$, the relevant constraints on these parameters are those which pertain to spin-dependent scattering. Several direct-detection experiments already provide comparable, stringent limits on spin-dependent scattering [23,30,31]. Moreover, the next generation of these experiments, including COUPP-60 and PICO-250L, are projected to significantly extend the reach of these experiments in the near future [32]. In this paper, our primary aim is to investigate the sensitivity of these latter experiments to scalar-pseudoscalar interactions between dark-matter particles and atomic nuclei. We therefore focus on the results from COUPP-4, for which the experimental setup and analysis parallel those for COUPP-60 and PICO-250L, when discussing existing limits on spin-dependent scattering. These limits are typically expressed as bounds on the spin-dependent dark-matter/proton scattering cross section $\sigma_{\chi p}^{(\mathrm{AA})}$ for a dark-matter particle whose interactions with nuclei are primarily due to the axial-vector operators $\mathcal{O}_{\chi q}^{(\mathrm{AA})}$. This cross section may be parametrized as

$$\sigma_{\chi p}^{(\mathrm{AA})} = \frac{3 a_{\chi p}^2 \mu_{\chi p}^2}{\pi \Lambda^4}, \quad (4.8)$$

where μ_p is the reduced mass of the χ/proton system and where

$$a_{\chi N} \equiv \sum_{q=u,d,s} c_q^{(\mathrm{AA})} \Delta q^{(N)} \quad (4.9)$$

are the axial-vector analogues of the χ/nucleon couplings $g_{\chi N}$ given in Eq. (2.20). Note that because we take χ to be a

Dirac fermion, this expression differs by a factor of 4 from the standard expression for a Majorana fermion. The differential cross section for χ/nucleus scattering for such an interaction, expressed in terms of $\sigma_{\chi p}^{(\mathrm{AA})}$, is given by

$$\frac{\partial\sigma_{\chi T}^{(\mathrm{AA})}}{\partial E_R} = \frac{2\sigma_{\chi p}^{(\mathrm{AA})} m_T}{3\mu_p^2 v^2}\frac{J_T+1}{J_T} \times \left(\langle S_p\rangle + \frac{a_{\chi n}}{a_{\chi p}}\langle S_n\rangle\right)^2 F^2(E_R). \tag{4.10}$$

It is therefore straightforward to convert the limits on $\sigma_{\chi p}^{(\mathrm{AA})}$ into limits on the expected event rate for dark-matter scattering off nuclei within the detector volume. The latter limits are model-independent and applicable to any interaction between dark-matter and atomic nuclei, including the scalar-pseudoscalar interactions which are the focus of this paper.

The bounds implied by COUPP-4 data on the parameter space of each of our three coupling scenarios, along with the projected reach into that parameter space for both COUPP-60 and PICO-250L, will be discussed in the next section. These bounds and sensitivities will be expressed as contours in (m_χ, M_*) space for each scenario and for several benchmark values of θ, where M_* denotes the corresponding suppression scale M_{I}, M_{II}, or M_{III}. In evaluating these contours, we will make use of the DMFormFactor package [29]. We will also include bands indicating the uncertainties in these contours which arise as a result of the uncertainties in the nucleon couplings $g_{\chi N}$ discussed in Sec. II.

B. Relic abundance

Thermal freeze-out is a natural mechanism through which a sizable relic abundance can be generated for a massive particle with suppressed couplings to SM states. It is therefore useful to identify the regions of parameter space within which the relic abundance of a dark-matter particle which annihilates via the $\mathcal{O}_{\chi q}^{(\mathrm{SP})}$ operator reproduces the observed dark-matter relic abundance $\Omega_{\mathrm{DM}} \approx 0.26$ [33]. In this section, we briefly summarize the relic-abundance calculation for an interaction of this sort. Note that we take χ to be a Dirac fermion throughout and make use of the general formalism in Ref. [34] for multiparticle freeze-out dynamics in order to evaluate the total relic abundance of χ and its conjugate $\bar{\chi}$, which in this case represent distinct degrees of freedom.

The evolution of the total number density $Y \equiv Y_\chi + Y_{\bar{\chi}}$ of particles which contribute to the dark-matter abundance at late times due to thermal freeze-out in this scenario can be described by the single differential equation

$$\frac{dY}{dt} = -s\langle\sigma|v|\rangle[Y^2 - (Y^{\mathrm{eq}})^2], \tag{4.11}$$

where Y^{eq} is the value which Y would have were χ and $\bar{\chi}$ in thermal equilibrium at time t; where $s = 2\pi^2 g_{*s}(T)T^3/45$ is the entropy density of the universe, expressed here in terms of the temperature T of the thermal bath at time t and the number of effectively massless degrees of freedom $g_*(T)$ at that temperature T; and where $\langle\sigma|v|\rangle$ is the thermally averaged total cross section for dark-matter annihilation. The total present-day dark-matter-abundance contribution from χ and $\bar{\chi}$ due to thermal freeze-out is related to the present-day value Y_{now} of Y by

$$\Omega_\chi \equiv \frac{\rho_\chi}{\rho_{\mathrm{crit}}} = \frac{s_{\mathrm{now}} m_\chi Y_{\mathrm{now}}}{\rho_{\mathrm{crit}}}, \tag{4.12}$$

where $s_{\mathrm{now}} \approx 2.22\times10^{-38}\,\mathrm{GeV}^3$ and $\rho_{\mathrm{crit}} \approx 4.18\times10^{-47}\,\mathrm{GeV}^4$ are the present-day entropy density and present-day critical energy density of the universe, respectively.

In the case in which χ and $\bar{\chi}$ annihilate primarily to SM quarks via $\mathcal{O}_{\chi q}^{(\mathrm{SP})}$, we find that the thermally averaged annihilation cross section for processes of the form $\bar{\chi}\chi \to \bar{q}q$ is given by

$$\langle\sigma|v|\rangle = \frac{3x}{256\pi m_\chi^5 K_2(x)}\sum_q \frac{c_q^2}{\Lambda^4}\mathcal{I}_q(x), \tag{4.13}$$

where we have defined

$$\mathcal{I}_q(x) \equiv \int_{4m_\chi^2}^{\infty} ds\sqrt{s(s-4m_\chi^2)^3(s-4m_q^2)}K_1\left(\frac{x\sqrt{s}}{m_\chi}\right). \tag{4.14}$$

In these expressions, $x \equiv m_\chi/T$, $s = (p_\chi + p_{\bar{\chi}})^2$ is the usual Mandelstam variable (*not* the entropy density of the universe, and *not* the strange quark either), and $K_1(x)$ and $K_2(x)$ denote the modified Bessel functions of the second kind of degree one and two, respectively.

In the next section we will display contours corresponding to the condition $\Omega_\chi = \Omega_{\mathrm{DM}}$, as well as contours of $\langle\sigma|v|\rangle$. In accord with expectation, we will find that a relic abundance of the correct order is obtained for $\langle\sigma|v|\rangle \approx 1$ pb. In interpreting these results, it should be noted that Ω_χ depends on m_χ in the usual manner, whereas this quantity depends on θ and the corresponding suppression scale M_{I}, M_{II}, or M_{III} in each of our coupling scenarios through the ratio c_q^2/Λ^4 in Eq. (4.13). Generally speaking, $\Omega_\chi \propto \langle\sigma|v|\rangle^{-1}$ for thermal freeze-out, and therefore a higher suppression scale corresponds to a smaller $\langle\sigma|v|\rangle$ and a larger relic abundance.

C. Collider constraints

Colliders offer a complementary way of probing the couplings between dark-sector and visible-sector fields. In particular, the effective operators given in Eq. (2.1) generically contribute to the event rate for processes of the form

$pp \to X + E_T$ at the LHC—i.e., so-called "mono-anything" processes—where X denotes a single SM particle such as a photon (the monophoton channel), an electroweak gauge boson, or even a "particle" such as a hadronic jet (the monojet channel). While the results depend on the particular operator and the relative values of the coupling coefficients (see, e.g., Ref. [35]), the most stringent constraints on such operators are typically those derived from limits on monojet production at ATLAS [36,37] and CMS [38,39] and from limits on the production of a hadronically decaying $W^{\pm}$ or Z boson at ATLAS [40]. We will henceforth focus on these channels, but we also note that a combined analysis [41,42] involving all relevant $pp \to X + E_T$ processes would lead to a slight enhancement of the bounds from these two leading channels individually. Moreover, we also note that searches in the mono-b and $t\bar{t} + E_T$ channels can potentially supersede these limits for models in which the couplings between the dark matter and the third-generation quarks are enhanced [28], as is the case in our Scenario II.

We now proceed to derive a set of rough limits on the corresponding suppression scale $M_{\rm I}$, $M_{\rm II}$, or $M_{\rm III}$ associated with each of our benchmark coupling scenarios. We derive these limits under the assumption that a contact-operator description of the interactions between χ and the SM quarks remains valid up to the center-of-mass-energy scale $\sqrt{s} \approx 8$ TeV of the LHC. We then return to discuss how these results are altered in cases in which the contact-operator description is valid at scales relevant for direct detection, but breaks down at scales well below $\sqrt{s}$.

We begin by noting that the monojet [39] and mono-W/Z [40] analyses which correspond to the most stringent current limits on dark-matter production at the LHC are effectively counting experiments which serve to constrain the total cross section for the corresponding production processes. A lower limit $M_* > M_{\rm min}$ on the heavy mass scale M_* defined for the operator D3 in the standard operator-classification scheme of Ref. [43] [which corresponds to our scalar-pseudoscalar operator $\mathcal{O}_{\chi q}^{(\rm SP)}$] from either of these analyses corresponds to a limit $M_{\rm II} > M_{\rm min}/2^{1/6}$ in our Scenario II with $\theta = \pi/4$. We also note that the production cross section for each process scales like $\sigma_{\rm I}(m_\chi, M_{\rm I}, \theta) \propto M_{\rm I}^{-4}$ in Scenario I, whereas it scales like $\sigma_{\rm II,III}(m_\chi, M_{\rm II,III}, \theta) \propto M_{\rm II,III}^{-6}$ in Scenarios II and III. It therefore follows that bounds on $M_{\rm I}$ can be derived from the bounds on $M_{\rm min}$ quoted in Refs. [39,40] and the ratio of the corresponding production cross sections for the same m_χ and the same fiducial value of $M_{\rm I}$. In this analysis, we choose 1 TeV as our fiducial mass scale. We therefore have

$$\frac{M_{\rm I}}{\rm GeV} \gtrsim \left[\frac{\sigma_{\rm I}(m_\chi, 1\ {\rm TeV}, \theta)}{2\sigma_{\rm II}(m_\chi, 1\ {\rm TeV}, \pi/4)}\right]^{1/4} \left(\frac{M_{\rm min}}{10\ {\rm GeV}}\right)^{3/2}. \quad (4.15)$$

Likewise, lower limits on $M_{\rm II}$ and $M_{\rm III}$ may be derived using the relation

$$M_{\rm II,III} \gtrsim \left[\frac{\sigma_{\rm II,III}(m_\chi, 1\ {\rm TeV}, \theta)}{2\sigma_{\rm II}(m_\chi, 1\ {\rm TeV}, \pi/4)}\right]^{1/6} M_{\rm min}. \quad (4.16)$$

Constraint contours corresponding to the limits on contact-operator interactions from these most recent monojet and mono-W/Z analyses will be discussed in the next section for each of our three coupling scenarios. The relevant cross sections in each case are evaluated at parton level using the MadGraph/MadEvent package [44] (with the CTEQ6L1 PDF set [45]) including the contribution from processes involving b quarks in the initial state. The event-selection criteria we employ in estimating these limits are modeled on those described in Ref. [39] for the monojet channel and Ref. [40] for the mono-W/Z channel, and we have verified that minor alterations in these cuts do not have significant effects on our results.

As mentioned above, it is important to note that constraints derived in this manner are valid only in the regime in which interactions between dark-matter particles and SM quarks can legitimately be modeled as contact operators at energies comparable to $\sqrt{s}$. In other words, they are valid for processes in which the mass m_ϕ of the particle ϕ which mediates the interaction is much larger than the momentum transfer to the dark-matter system. By contrast, for lower mediator masses $m_\phi \lesssim 1$ TeV, these limits are no longer applicable—even for $m_\phi > m_\chi$. Constraints on interactions between dark-matter particles and SM quarks can still be derived from LHC data for theories in which $m_\phi \lesssim 1$ TeV; however, such constraints are highly model dependent, sensitive to the full structure of the dark sector, and frequently weaker than the naïve limits one would obtain for these same channels in the contact-operator regime [46].

On the other hand, while the contact-operator approximation becomes unreliable from the perspective of collider phenomenology for $m_\phi \lesssim 1$ TeV, it remains valid for direct-detection phenomenology down to far lower values of m_ϕ. Indeed, interactions involving light mediators can still be reliably modeled as contact interactions at energies relevant for direct detection, provided that $m_\phi \gtrsim 1$ GeV. Moreover, the relic-density calculation in Sec. IV B also remains qualitatively unaltered in the presence of a light mediator down to the kinematic threshold $m_\phi = m_\chi$. Below this threshold, annihilation into pairs of on-shell mediators becomes kinematically accessible. Moreover, below this threshold, the behavior of the thermally averaged annihilation cross section transitions from $\langle\sigma|v|\rangle \propto m_\chi^2/m_\phi^4$ to $\langle\sigma|v|\rangle \propto 1/m_\chi^2$ because m_χ is always the dominant energy scale entering into the propagators for all diagrams contributing to this annihilation cross section. Above this kinematic threshold, by contrast, we find that the correct relic density can be obtained for perturbative couplings between ϕ and both the dark-sector and visible-sector fermions in our theory, provided that $m_\chi \lesssim \mathcal{O}(10\ {\rm TeV})$.

In light of these considerations, we emphasize that the monojet and mono-W/Z limits we have discussed here

should not be interpreted as exclusion bounds, but rather as relations which indicate the regions within which LHC data can be interpreted as requiring that the mediator particle(s) ϕ not be particularly heavy. Indeed, the suppression scale $M_{\rm I}$, $M_{\rm II}$, or $M_{\rm III}$ in each of our three coupling scenarios can still be large even if m_ϕ is light, provided the coupling between ϕ and either χ or the SM quarks is small.

V. RESULTS

In the previous section, we outlined the physics that determines the reach of various direct-detection experiments, assuming only pseudoscalar interactions between dark matter and Standard-Model quarks. We also outlined the physics that determines the cosmological dark-matter abundances after freeze-out, and summarized the physics that determines the reach of monojet and mono-W/Z searches at the LHC. As we saw in Sec. IV, all of these calculations depend to varying degrees on the particular flavor coupling structure assumed (i.e., whether we are operating within Scenario I, Scenario II, or Scenario III), and on the particular value of θ in each case.

The results of these analyses are shown in Fig. 2. The reaches of the current and future direct-detection experiments considered in this study are shown in red, purple, and blue (along with their associated uncertainties); for the COUPP-60 experiment we have assumed an exposure of 10^5 kg d while for the PICO-250L experiment we have assumed three years of running with a 500 kg fiducial mass [32]. Likewise, the black contour in each case corresponds to the condition $\Omega_\chi = \Omega_{\rm DM}$, which one would naïvely expect to occur for $\langle\sigma|v|\rangle \approx 1$ pb. The orange dashed curve, by contrast, explicitly indicates the points for which $\langle\sigma|v|\rangle = 1$ pb, and the peach-colored and yellow-colored bands around it correspond to the regions within which the annihilation cross section matches this value to within an increasing number of powers of ten (i.e., 0.1 pb $\leq \langle\sigma|v|\rangle \leq$ 10 pb and 0.01 pb $\leq \langle\sigma|v|\rangle \leq$ 100 pb, respectively). Finally, the blue dashed curve and cyan dot-dashed curve respectively indicate the lower limits on $M_{\rm I}$, $M_{\rm II}$, or $M_{\rm III}$ from monojet and mono-W/Z searches at the LHC in the case of a heavy mediator.

Note that we have included the abundance and collider curves within these plots merely in order to provide guidance when interpreting the impact of the direct-detection curves, and to indicate regions of specific interest. In particular, the collider and abundance curves do not represent strict bounds in any sense. For example, within each panel of Fig. 2, the region of the (m_χ, M_*) plane *below* the $\Omega_\chi \sim \Omega_{\rm DM}$ contour (with M_* representing either $M_{\rm I}$, $M_{\rm II}$, or $M_{\rm III}$, as appropriate) is actually consistent with observational limits under the assumption that some additional contribution makes up the remainder of $\Omega_{\rm DM}$. Conversely, the region *above* this contour can also be consistent with a thermal relic dark-matter candidate if the branching fraction for dark-matter annihilation into visible-sector particles is less than unity due to the presence of additional annihilation channels. This will also be true if an additional source of entropy production dilutes the relic abundance after freeze-out. Moreover, as discussed in Sec. IV B, the abundance-related orange and black curves in Fig. 2 do not represent true relic-density limits if $m_\phi < m_\chi$. Similarly, as discussed in Sec. IV, our monojet and mono-W/Z collider curves only represent exclusion bounds under the assumption that the contact-operator description of our scalar/pseudoscalar interaction remains valid up to the TeV scale. When this is not the case, the bounds can be far weaker or even effectively disappear.

As we see from Fig. 2, the dark-matter abundance does not depend significantly on the value of θ in Scenarios I or III. By contrast, in Scenario II, our results depend sensitively on θ due to the enhanced couplings to third-generation quarks relative to those of the first and second generations. Indeed, in Scenario II the abundance contours have sharp kinks or discontinuities that are not apparent in Scenarios I or III. This behavior ultimately arises because the couplings to the SM quarks in Scenario II are proportional to their masses, leading to a dramatic enhancement in the annihilation rate when the thresholds for new annihilation channels into heavy quark species are crossed. However, this assumes that the dark-matter coupling to these heavy-quark species is substantial—a feature that is ultimately θ dependent.

Overall, examining the plots in Fig. 2, we see that there are three main conclusions which may be drawn. The first and most significant result demonstrated in Fig. 2 is that there are regions of parameter space for which a thermal abundance matching $\Omega_{\rm DM}$ is not only consistent with current experimental limits on the pseudoscalar operator, but can actually be probed by the next generation of direct-detection experiments. This does not occur in merely one or two fine-tuned cases, but rather as a fairly generic result for all three scenarios defined in Sec. II and for most values of θ.

Second, we observe that in some cases, the opposite is true: the reach of our direct-detection experiments is significantly less than might be expected based on the magnitudes of the $\Delta\tilde{q}^{(N)}$ coefficients. This is particularly true for the $\theta = \pi/4$ case of Scenario I, or the $\theta = 0$ case of Scenario II. Indeed, in such cases, we see that the direct-detection experiments cannot even probe that portion of the parameter space that would be associated with a thermal relic. Moreover, we see from Fig. 2 that the uncertainties in these cases are sufficiently broad that the direct-detection experiments may not even have any significant reach at all! Ultimately, these effects can easily be understood in relation to Fig. 1, where we have seen that for both of these cases the effective dark-matter/nucleon couplings themselves come extremely close to vanishing. (A similar thing would also have happened for $\theta \approx \pi/8$ in Scenario III, if such a θ value were being plotted in Fig. 2.) As discussed

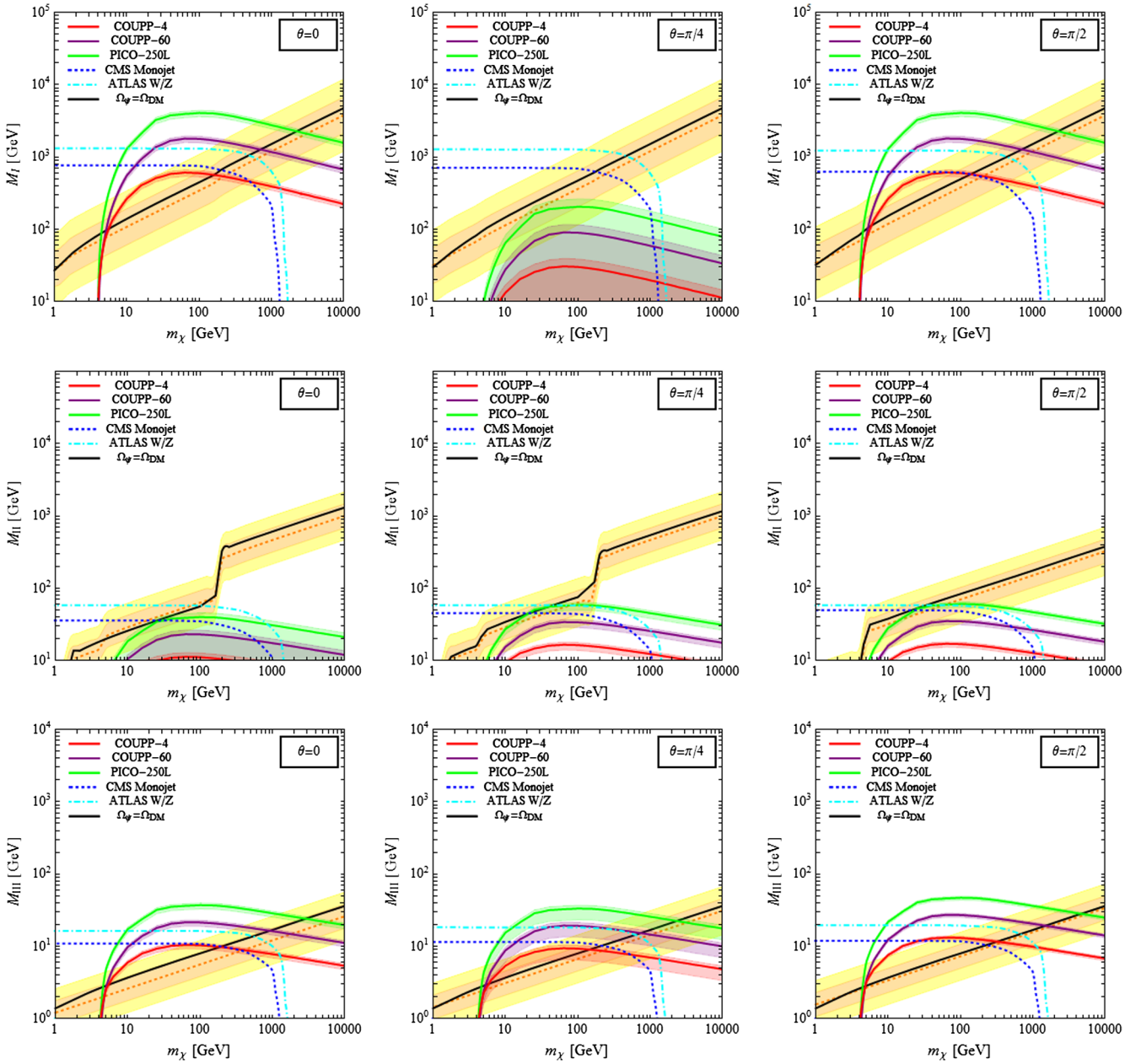

FIG. 2 (color online). Experimental reach of direct-detection experiments, assuming pseudoscalar interactions with the benchmark coupling structures of our Scenario I (top row), Scenario II (center row), and Scenario III (bottom row), with $\theta = 0$ (left column), $\theta = \pi/4$ (center column), and $\theta = \pi/2$ (right column) in each case. These coupling structures are discussed in Sec. II C, and each panel is plotted as a function of the dark-matter mass m_χ and the mass scale $M_{\rm I}$, $M_{\rm II}$, or $M_{\rm III}$ associated with the corresponding scenario. Within each panel, the red curve indicates the upper limit of the region already excluded by COUPP-4 data, while the purple and green curves respectively indicate the projected discovery reaches of the COUPP-60 and PICO-250L experiments. The thickness of each curve indicates the uncertainty associated with the corresponding experimental reach, as discussed and calculated in the text; note that in some cases these uncertainties are sufficiently large as to cause these "lines" to become entire red-, purple-, and blue-shaded regions. For guidance, we have also indicated the contour (black line) along which $\Omega_\chi = \Omega_{\rm DM} \approx 0.26$, while the orange dashed line corresponds to a thermally averaged dark-matter annihilation cross section $\langle\sigma|v|\rangle = 1$ pb. The pale peach- and yellow-colored bands correspond to the regions within which 0.1 pb $\leq \langle\sigma|v|\rangle \leq 10$ pb and 0.01 pb $\leq \langle\sigma|v|\rangle \leq 100$ pb, respectively. Finally, the blue dashed curve and cyan dot-dashed curve respectively indicate the lower limits on the appropriate mass scale $M_{\rm I,II,III}$ from monojet and mono-W/Z searches at the LHC which would apply in the case of a heavy mediator. We see from these plots that there are many situations in which upcoming direct-detection experiments can easily reach into the range of greatest interest for thermally produced dark matter and its possible collider signatures—even when only pseudoscalar interactions between dark matter and Standard-Model quarks are assumed.

in Sec. II, these are situations in which the dark matter couples significantly to quarks, but not to nucleons. In such cases, we conclude that the nonobservation of a dark-matter signal in COUPP-4 and in future direct-detection experiments need not rule out the existence of dark matter which nevertheless still couples to quarks and which could therefore potentially produce a signal at collider experiments.

Finally, conversely, we see that the effects of isospin violation (i.e., variations in the value of θ) can have dramatic effects, potentially enhancing the reach of direct-detection experiments quite significantly compared with the reach of these experiments when nucleon-level isospin symmetry is preserved. For example, in Scenario I, we note that the reach of PICO-250L is approximately 20 times greater (in terms of the values of $M_{\rm I}$ being probed) for $\theta = 0$ than for $\theta = \pi/4$.

VI. CONCLUSIONS

In this paper, we have studied the sensitivity of direct-detection experiments to dark matter which couples to quarks through dimension-six effective operators of the form $\mathcal{O}_{\chi q}^{(\rm SP)} \sim c_q(\bar{\chi}\chi)(\bar{q}i\gamma^5 q)$, utilizing (for illustrative purposes) several distinct benchmark choices for the quark couplings c_q. As we discussed, such effective operators give rise to velocity-suppressed spin-dependent dark-matter/nucleon scattering. Such operators can also give rise to $\bar{\chi}\chi \to \bar{q}q$ annihilation from a p-wave initial state, as well as mono-anything signals at the LHC.

Although it might naïvely be supposed that velocity-dependent spin-dependent scattering would produce an unobservably small event rate at direct-detection experiments, we have demonstrated that this in fact need not be the case. Indeed, as we have seen, the velocity-suppression factors that arise in the pseudoscalar matrix element can be compensated by extra enhancement factors which also emerge in the pseudoscalar case when relating the corresponding pseudoscalar quark currents to effective pseudoscalar nucleon currents. These latter enhancement factors are of size $\mathcal{O}(10^2$–$10^3)$ relative to similar factors associated with velocity-*independent* spin-dependent scattering (such as arises through axial-vector interactions). As a result, contrary to popular lore, we see that velocity-suppressed scattering may actually be within reach of current and upcoming direct-detection experiments. This then necessitates a sensitivity study of the sort that we have performed.

Specifically, our main conclusions are as follows:

- We have shown that there exists a substantial region of $(m_\chi, M_{\rm I,\,II,\,III}, \theta)$ parameter space in which the couplings of the $\mathcal{O}_{\chi q}^{(\rm SP)}$ operators are consistent with a thermal relic density which matches observation. Of course, given the model-independent nature of our approach, we have not addressed the question of how these operators might ultimately be embedded in a UV-complete model. Nevertheless, such models can easily be constructed—for example, the coupling structure of Scenario II can be realized within the context of CP-violating two-Higgs-doublet models [47].
- A subset of the above parameter space is excluded by current bounds from COUPP-4, and it is expected that an even larger region of this viable parameter space will be probed by COUPP-60 and PICO-250L.
- While part of the parameter space may be constrained by LHC bounds if the contact-operator approximation remains valid at the TeV scale, there are a wide range of models for which spin-dependent scattering is actually the discovery channel. As we have seen, this is true because the velocity-suppression effects normally associated with pseudoscalar couplings can be overcome through nucleonic effects that emerge in relating quark pseudoscalar currents to nucleon pseudoscalar currents.
- Conversely, there are special situations (often associated with isospin-preserving limits) in which these same nucleonic effects render direct-detection experiments utterly insensitive to nonzero couplings between dark matter and SM quarks. In other words, we have seen that dark matter can have a significant, nonvanishing coupling to quarks and yet simultaneously have no coupling to nucleons! This opens up the intriguing possibility that collider experiments and other indirect-detection experiments could potentially see dark-matter signals to which direct-detection experiments would be utterly blind. This may be extremely relevant in case of future apparent conflicts between positive signals from collider experiments and negative results from direct-detection experiments.
- Finally, we see that isospin *violation* generally tends to *enhance* dark-matter signals in direct-detection experiments relative to the signals which would have been expected if the quark/nucleon couplings were isospin-preserving. Moreover, for pseudoscalar couplings, this enhancement is not just a factor of 2 or 3 (as would be the case for axial-vector interactions), but a factor of 10 or more. This then opens up the possibility that direct-detection experiments can be sensitive to such pseudoscalar couplings.

A few comments are in order, especially in relation to the last two points above. In Scenario I, dark-matter/nucleon couplings are maximally isospin-violating when $\theta \approx 0$ or $\theta = \pi/2$. Interestingly, these cases provide the greatest sensitivity for direct-detection experiments (such as PICO-250L) which are sensitive to spin-dependent scattering. By contrast, detectors which are only sensitive to spin-independent scattering would have no chance of discovering such events, even if velocity-dependent effects are included. This is because, as discussed in Sec. II, all terms originating from $\mathcal{O}_{\chi q}^{(\rm SP)}$ which contribute to the scattering

cross section—and not just those at leading order—are spin dependent.

On the other hand, we have seen that the sensitivity of direct-detection experiments is especially poor in the isospin-conserving cases (such as $\theta \approx \pi/4$ in our Scenario I) for which the couplings to up and down quarks are similar. This poor sensitivity is ultimately the result of a destructive interference among these quark-level couplings, resulting in a small net coupling to both protons and neutrons. Indeed, in the limit within Scenario I for which $m_{u,d} \ll m_s$ and $\Delta\tilde{G}^{(N)} \sim 0$, we find $g_{\chi p}$, $g_{\chi n} \to 0$ identically at $\theta = \pi/4$. Note that result is detector independent: one obtains a large suppression in the event rate *regardless* of whether the detector is sensitive to spin-dependent scattering from protons or neutrons. Moreover, since the dark-matter bilinear is a scalar, dark-matter annihilation is p-wave suppressed. Thus, although the annihilation rate at the time of freeze-out may have been large enough to ensure the correct relic density, the annihilation cross section at the current epoch would be so small as to be unobservable. Dark-matter models of this sort would be difficult to probe via any direct- or indirect-detection experiments.

In this paper, we considered three different scenarios for the couplings c_q between the dark matter and SM quarks. These correspond to different weightings for the various contributions from the light quarks to the resulting dark-matter/nucleon couplings and their associated dark-matter scattering rates. In Scenario I, for example, the dominant contributions came from the couplings of the quarks of the first generation, but we found that there also exist small contributions from the strange quark and heavier quarks. Likewise, in Scenario I we found that $g_{\chi p}$, $g_{\chi n} \to 0$ for $\theta = \pi/4$. In Scenario III, by contrast, the additional contributions from the strange and heavier quarks are absent. Moreover, since the c_q coefficients of Scenario III scale with the masses of the quarks, we instead find that $g_{\chi p}$, $g_{\chi n} \to 0$ for $\tan\theta = m_u/m_d$. In this connection, it is perhaps worth emphasizing that it is only for the pseudoscalar interactions that there exist values of θ for which both $g_{\chi p}$ and $g_{\chi n}$ vanish simultaneously. As can be seen in Fig. 1, this does not happen for any of the analogous couplings in the axial-vector case.

Finally, Scenario II is an example of a class of models in which the largest dark-matter coupling is to the strange quark or the heavy quarks. As discussed earlier, this particular example is motivated by minimal flavor violation. As evident from Fig. 2, the sensitivity of direct-detection experiments to viable dark-matter models is suppressed for such cases. It is clear why this occurs. In Scenario II, the largest dark-matter couplings are those to the second- and third-generation quarks—indeed, these are ultimately bounded by constraints on the relic density. Unfortunately, the contributions from these second- and third-generation quark couplings to dark-matter scattering are relatively small as a result of a suppression of the corresponding nucleon enhancement factors, while the coupling to first-generation quarks is necessarily small by assumption in this scenario.

Depending on the details of the short-distance (ultraviolet) physics model we imagine, dark matter which couples to quarks through an effective operator such as $\mathcal{O}_{\chi q}^{(\mathrm{SP})}$ may also be amenable to mono-anything searches at the LHC. In particular, for isospin-conserving variants in which the first-generation quarks dominate the scattering, LHC searches may be the only viable options for discovery. Moreover, LHC sensitivity may be enhanced for flavor structures such as those in Scenario II which are motivated by minimal flavor violation, due to the large contribution to the LHC event rate that arises from the couplings to the heavy quarks. Ultimately, however, LHC sensitivity depends on the details of the model, and in particular on the flavor structure of the couplings. For the wide class of models in which such large LHC event rates do not occur, spin-dependent direct detection will then be the discovery search channel.

ACKNOWLEDGMENTS

We would like to thank Z. Chacko, D. Marfatia, D. Sanford, W. Shepherd, M. Sher, X. Tata, and U. van Kolck for useful discussions. K. R. D., J. K., and B. T. would also like to thank the Kavli Institute for Theoretical Physics (KITP) in Santa Barbara, the Galileo Galilei Institute for Theoretical Physics (GGI) in Florence, Italy, and the Center for Theoretical Underground Physics and Related Areas (CETUP*) in South Dakota for their hospitality during various stages of the completion of this work. J. K. and B. T. would also like to acknowledge these institutions for partial support during these periods. K. R. D. is supported in part by the Department of Energy under Grants No. DE-FG02-04ER-41298 and No. DE-FG02-13ER-41976, and was also supported in part by the National Science Foundation through its employee IR/D program through August 2013. The work of J. K. before June 1, 2013 was supported in part by Department of Energy Grant No. DE-FG02-04ER41291, while the work of J. K. after June 15, 2013 is supported in part by NSF CAREER Award PHY-1250573. B. T. is supported in part by DOE Grant No. DE-FG02-04ER-41291 and in part by the Natural Sciences and Engineering Research Council of Canada. D. Y. is supported in part by DOE Grants No. DE-FG02-04ER-41291 and No. DE-FG02-13ER-42024. The opinions and conclusions expressed herein are those of the authors, and do not represent either the Department of Energy or the National Science Foundation.

[1] M. W. Goodman and E. Witten, Phys. Rev. D **31**, 3059 (1985).

[2] G. Jungman, M. Kamionkowski, and K. Griest, Phys. Rep. **267**, 195 (1996).

[3] D. Hooper, arXiv:0901.4090; N. Weiner, "Dark Matter Theory," video of lectures given at TASI 2009, http://physicslearning2.colorado.edu/tasi/tasi_2009/tasi_2009.htm; J. L. Feng, Annu. Rev. Astron. Astrophys. **48**, 495 (2010); R. W. Schnee, arXiv:1101.5205.

[4] J. D. Lewin and P. F. Smith, Astropart. Phys. **6**, 87 (1996).

[5] P. J. Fox and E. Poppitz, Phys. Rev. D **79**, 083528 (2009).

[6] See, e.g., D. Tucker-Smith and N. Weiner, Phys. Rev. D **64**, 043502 (2001); **72**, 063509 (2005); T. Hur, H. S. Lee, and S. Nasri, Phys. Rev. D **77**, 015008 (2008); J. L. Feng and J. Kumar, Phys. Rev. Lett. **101**, 231301 (2008); H. S. Cheon, S. K. Kang, and C. S. Kim, Phys. Lett. B **675**, 203 (2009); **698**, 324(E) (2011); S. Chang, G. D. Kribs, D. Tucker-Smith, and N. Weiner, Phys. Rev. D **79**, 043513 (2009); K. M. Zurek, Phys. Rev. D **79**, 115002 (2009); B. Batell, M. Pospelov, and A. Ritz, Phys. Rev. D **79**, 115019 (2009); S. Profumo, K. Sigurdson, and L. Ubaldi, J. Cosmol. Astropart. Phys. 12 (2009) 016; F. Chen, J. M. Cline, and A. R. Frey, Phys. Rev. D **80**, 083516 (2009); I. Cholis and N. Weiner, arXiv:0911.4954; X. Gao, Z. Kang, and T. Li, Eur. Phys. J. C **69**, 467 (2010); D. Feldman, Z. Liu, P. Nath, and G. Peim, Phys. Rev. D **81**, 095017 (2010); P. T. Winslow, K. Sigurdson, and J. N. Ng, Phys. Rev. D **82**, 023512 (2010); J. L. Feng, M. Kaplinghat, and H.-B. Yu, Phys. Rev. D **82**, 083525 (2010); M. Aoki, M. Duerr, J. Kubo, and H. Takano, Phys. Rev. D **86**, 076015 (2012); D. Chialva, P. S. B. Dev, and A. Mazumdar, Phys. Rev. D **87**, 063522 (2013); S. Bhattacharya, A. Drozd, B. Grzadkowski, and J. Wudka, J. High Energy Phys. 10 (2013) 158;

[7] K. R. Dienes and B. Thomas, Phys. Rev. D **85**, 083523 (2012); **85**, 083524 (2012); K. R. Dienes, J. Kumar, and B. Thomas, Phys. Rev. D **86**, 055016 (2012).

[8] J. R. Ellis, K. A. Olive, and C. Savage, Phys. Rev. D **77**, 065026 (2008).

[9] M. A. Shifman, A. I. Vainshtein, and V. I. Zakharov, Phys. Lett. B **78**, 443 (1978).

[10] R. L. Jaffe and A. Manohar, Nucl. Phys. **B337**, 509 (1990).

[11] J. Engel, S. Pittel, and P. Vogel, Int. J. Mod. Phys. E **1**, 1 (1992).

[12] P. Agrawal, Z. Chacko, C. Kilic, and R. K. Mishra, arXiv:1003.1912.

[13] J. Fan, M. Reece, and L.-T. Wang, J. Cosmol. Astropart. Phys. 11 (2010) 042.

[14] M. Freytsis and Z. Ligeti, Phys. Rev. D **83**, 115009 (2011).

[15] J. Kumar and D. Marfatia, Phys. Rev. D **88**, 014035 (2013).

[16] B. Adeva *et al.* [Spin Muon (SMC) Collaboration], Phys. Lett. B **369**, 93 (1996); **420**, 180 (1998).

[17] A. Airapetian *et al.* (HERMES Collaboration), Phys. Rev. D **71**, 012003 (2005).

[18] M. Alekseev *et al.* (COMPASS Collaboration), Phys. Lett. B **660**, 458 (2008); **693**, 227 (2010).

[19] G. S. Bali *et al.* (QCDSF Collaboration), Phys. Rev. Lett. **108**, 222001 (2012).

[20] H.-Y. Cheng, Phys. Lett. B **219**, 347 (1989); H.-Y. Cheng and C. W. Chiang, J. High Energy Phys. 07 (2012) 009.

[21] Y. Bai, P. J. Fox, and R. Harnik, J. High Energy Phys. 12 (2010) 048.

[22] A. Kurylov and M. Kamionkowski, Phys. Rev. D **69**, 063503 (2004).

[23] E. Behnke*et al.* (COUPP Collaboration), Phys. Rev. D **86**, 052001 (2012).

[24] COUPP Collaboration (private communication).

[25] S. J. Brodsky, J. R. Ellis, and M. Karliner, Phys. Lett. B **206**, 309 (1988).

[26] J. Beringer *et al.* (Particle Data Group Collaboration), Phys. Rev. D **86**, 010001 (2012).

[27] K. R. Dienes, J. Kumar, B. Thomas, D. Yaylali *et al.*, in progress.

[28] T. Lin, E. W. Kolb, and L.-T. Wang, Phys. Rev. D **88**, 063510 (2013).

[29] N. Anand, A. L. Fitzpatrick, and W. C. Haxton, arXiv:1308.6288.

[30] M. Felizardo, T. A. Girard, T. Morlat, A. C. Fernandes, A. R. Ramos, J. G. Marques, A. Kling, J. Puibasset *et al.*, Phys. Rev. Lett. **108**, 201302 (2012).

[31] S. Archambault *et al.* (PICASSO Collaboration), Phys. Lett. B **711**, 153 (2012).

[32] R. Neilson, talk given at Aspen 2013, http://indico.cern.ch/getFile.py/access?contribId=69&sessionId=3&resId=0&materialId=slides&confId=197862.

[33] P. A. R. Ade *et al.* (Planck Collaboration), arXiv:1303.5076 [Astron. Astrophys. (to be published)].

[34] J. Edsjo and P. Gondolo, Phys. Rev. D **56**, 1879 (1997).

[35] A. Birkedal, K. Matchev, and M. Perelstein, Phys. Rev. D **70**, 077701 (2004); J. L. Feng, S. Su, and F. Takayama, Phys. Rev. Lett. **96**, 151802 (2006); M. Beltran, D. Hooper, E. W. Kolb, Z. A. C. Krusberg, and T. M. P. Tait, J. High Energy Phys. 09 (2010) 037; J. Goodman, M. Ibe, A. Rajaraman, W. Shepherd, T. M. P. Tait, and H.-B. Yu, Phys. Lett. B **695**, 185 (2011); P. J. Fox, R. Harnik, J. Kopp, and Y. Tsai, Phys. Rev. D **85**, 056011 (2012); J. Goodman and W. Shepherd, arXiv:1111.2359; Y. Bai and T. M. P. Tait, Phys. Lett. B **723**, 384 (2013).

[36] G. Aad *et al.* (ATLAS Collaboration), J. High Energy Phys. 04 (2013) 075.

[37] ATLAS Collaboration, Report No. ATLAS-CONF-2012-147.

[38] S. Chatrchyan *et al.* (CMS Collaboration), J. High Energy Phys. 09 (2012) 094.

[39] CMS Collaboration, Report No. CMS-PAS-EXO-12-048.

[40] G. Aad *et al.* (ATLAS Collaboration), Phys. Rev. Lett. **112**, 041802 (2014).

[41] K. Cheung, P.-Y. Tseng, Y.-L. S. Tsai, and T.-C. Yuan, J. Cosmol. Astropart. Phys. 05 (2012) 001.

[42] N. Zhou, D. Berge, and D. Whiteson, Phys. Rev. D **87**, 095013 (2013).

[43] J. Goodman, M. Ibe, A. Rajaraman, W. Shepherd, T. M. P. Tait, and H.-B. Yu, Phys. Rev. D **82**, 116010 (2010).

[44] J. Alwall, M. Herquet, F. Maltoni, O. Mattelaer, and T. Stelzer, J. High Energy Phys. 06 (2011) 128.

[45] J. Pumplin, D. R. Stump, J. Huston, H. L. Lai, P. M. Nadolsky, and W. K. Tung, J. High Energy Phys. 07 (2002) 012.

[46] H. An, X. Ji, and L.-T. Wang, J. High Energy Phys. 07 (2012) 182; H. An, R. Huo, and L.-T. Wang, Phys. Dark Univ. **2**, 50 (2013).

[47] See, e.g.: T. D. Lee, Phys. Rev. D **8**, 1226 (1973); G. C. Branco and M. N. Rebelo, Phys. Lett. B **160**, 117 (1985); S. Weinberg, Phys. Rev. D **42**, 860 (1990). For a review and further references, see G. C. Branco, P. M. Ferreira, L. Lavoura, M. N. Rebelo, M. Sher, and J. P. Silva, Phys. Rep. **516**, 1 (2012).